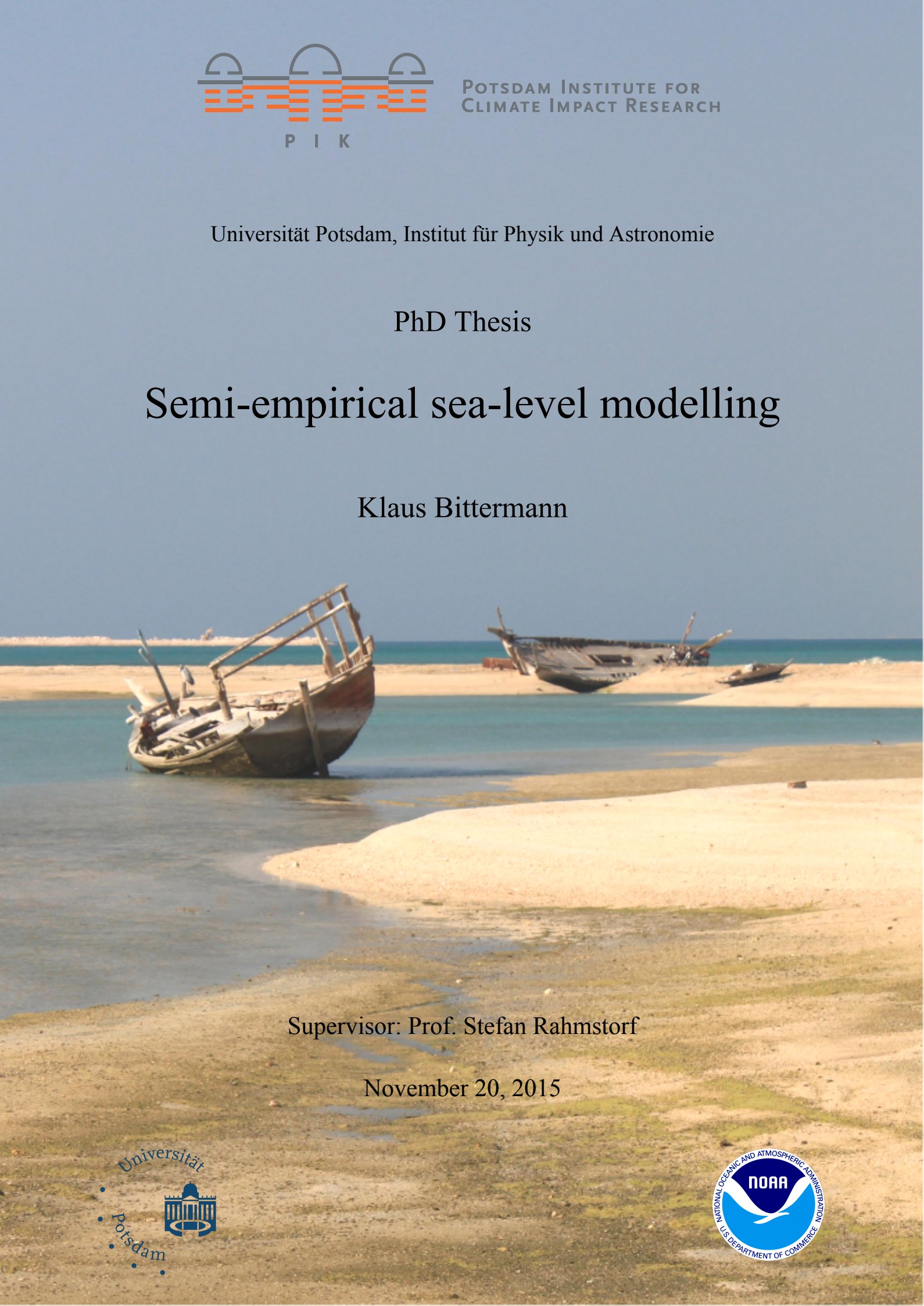

POTSDAM INSTITUTE FOR CLIMATE IMPACT RESEARCH

P I K

Universität Potsdam, Institut für Physik und Astronomie

PhD Thesis

Semi-empirical sea-level modelling

Klaus Bittermann

Supervisor: Prof. Stefan Rahmstorf

November 20, 2015

Universität Potsdam

NOAA NATIONAL OCEANIC AND ATMOSPHERIC ADMINISTRATION U.S. DEPARTMENT OF COMMERCE

Published online at the
Institutional Repository of the University of Potsdam:
URN urn:nbn:de:kobv:517-opus4-93881
http://nbn-resolving.de/urn:nbn:de:kobv:517-opus4-93881

Pure logical thinking cannot yield us any knowledge of the empirical world; all knowledge of reality starts from experience and ends with it.

Albert Einstein, 10 June 1933, University of Oxford

Abstract

Semi-empirical sea-level models (SEMs) exploit physically motivated empirical relationships between global sea level and certain drivers, in the following global mean temperature. This model class evolved as a supplement to process-based models (Rahmstorf (2007)) which were unable to fully represent all relevant processes. They thus failed to capture past sea-level change (Rahmstorf *et al.* (2012)) and were thought likely to underestimate future sea-level rise. Semi-empirical models were found to be a fast and useful tool for exploring the uncertainties in future sea-level rise, consistently giving significantly higher projections than process-based models.

In the following different aspects of semi-empirical sea-level modelling have been studied. Models were first validated using various data sets of global sea level and temperature. SEMs were then used on the glacier contribution to sea level, and to infer past global temperature from sea-level data via inverse modelling. Periods studied encompass the instrumental period, covered by tide gauges (starting 1700 CE (Common Era) in Amsterdam) and satellites (first launched in 1992 CE), the era from 1000 BCE (before CE) to present, and the full length of the Holocene (using proxy data). Accordingly different data, model formulations and implementations have been used.

It could be shown in Bittermann *et al.* (2013) that SEMs correctly predict 20th century sea-level when calibrated with data until 1900 CE. SEMs also turned out to give better predictions than the Intergovernmental Panel on Climate Change (IPCC) 4th assessment report (AR4, IPCC (2007)) models, for the period from 1961–2003 CE.

With the first multi-proxy reconstruction of global sea-level as input, estimates of the human-induced component of modern sea-level change and projections of future sea-level rise were calculated (Kopp *et al.* (2016)). It turned out with 90% confidence that more than 40 % of the observed 20th century sea-level rise is indeed anthropogenic. With the new semi-empirical and IPCC (2013) 5th assessment report (AR5) projections the gap between SEM and process-based model projections closes, giving higher credibility to both. Combining all scenarios, from strong mitigation to business as usual, a global sea-level rise of 28–131 cm relative to 2000 CE, is projected with 90%

confidence. The decision for a low carbon pathway could halve the expected global sea-level rise by 2100 CE.

Present day temperature and thus sea level are driven by the globally acting greenhouse-gas forcing. Unlike that, the Milankovich forcing, acting on Holocene timescales, results mainly in a northern-hemisphere temperature change. Therefore a semi-empirical model can be driven with northern-hemisphere temperatures, which makes it possible to model the main sub-component of sea-level change over this period. It showed that an additional positive constant rate of the order of the estimated Antarctic sea-level contribution is then required to explain the sea-level evolution over the Holocene. Thus the global sea level, following the climatic optimum, can be interpreted as the sum of a temperature induced sea-level drop and a positive long-term contribution, likely an ongoing response to deglaciation coming from Antarctica.

Sea Level, Climate Change, Projections, Anthropogenic Sea Level, Holocene, Semi-Empirical Models

Zusammenfassung

Semiempirische Meeresspiegelmodelle (SEMe) nutzen die physikalisch motivierte, empirische Beziehung des globalen Meeresspiegels zu einem bestimmten Antrieb. Im Folgenden ist das die mittlere globale Temperatur. Diese Modellklasse entstand als Ergänzung zu prozeßbasierten Modellen, die nicht alle relevanten Prozesse abbilden konnten (Rahmstorf (2007)) und die deshalb weder den beobachteten Meeresspiegel erklären konnten (Rahmstorf *et al.* (2012)) noch vertrauenswürdige Zukunftsprojektionen lieferten. Semiempirische Modelle sind eine gute und schnelle Option, die Unsicherheit im zukünftigen Meeresspiegelanstieg auszuloten, wobei sie konsistent höhere Zukunftsprojektionen lieferten als prozeßbasierte Modelle.

Im Folgenden wurden verschiedene Aspekte der semiempirischen Meeresspiegelmodellierung untersucht. Modelle wurden erst mit verschiedenen globalen Temperatur- und Meeresspiegeldatensätzen validiert. SEMe wurden dann auf den Meeresspiegelbeitrag von Gletschern angewandt und genutzt, um die globale Temperatur aus Meeresspiegeldaten abzuleiten. Die untersuchten Zeiträume variieren zwischen dem instrumentellen Abschnitt mit Pegelstandsmessungen (seit dem Jahr 1700 in Amsterdam) und Satellitendaten (seit 1992), dem Zeitraum seit 1000 vor Christus und dem gesamten Holozän (mittels Proxydaten). Entsprechend wurden verschiedene Daten, Modellformulierungen und -implementationen benutzt.

Es konnte in Bittermann *et al.* (2013) gezeigt werden, dass SEMe den beobachteten Meeresspiegel des 20sten Jahrhunderts korrekt vorhersagen können, wenn sie bis zum Jahr 1900 kalibriert wurden. Auch für den Zeitraum 1961 bis 2003 lieferten SEMe bessere Vorhersagen als der vierte Sachstandsbericht des Intergovernmental Panel on Climate Change (AR4, IPCC (2007)).

Mit der ersten globalen multi-proxy Rekonstruktion des globalen Meeresspiegels als Input konnten sowohl der anthropogene Anteil des modernen Meeresspiegelanstiegs als auch Zukunftsprojektionen berechnet werden (Kopp *et al.* (2016)). Es zeigt sich mit 90% Sicherheit, dass mehr als 40 % des beobachteten Meeresspiegelanstiegs im 20sten Jahrhundert anthropogenen Ursprungs sind. Mit den neuen semiempirischen Zukunftsprojektionen und denen des fünften Sachstandsberichtes (AR5) des IPCC (2013) läßt sich die Kluft zwischen SEMen und prozeßbasierten Modellen schließen, was beide

vertrauenswürdiger macht. Über alle Szenarien hinweg, von starker Treibhausgaseinsparung bis zum ungebremsten Ausstoß, ergibt sich, mit 90% Sicherheit, zwischen 2000 und 2100 ein Meeresspiegelanstieg von 28 bis 131 cm. Die Entscheidung starker Treibhausgaseinsparungen kann den erwarteten globalen Meeresspiegelanstieg im Jahr 2100 halbieren.

Die gegenwärtige globale Temperatur, und damit der globale Meeresspiegel, werden von dem global wirkenden Treibhausgasforcing bestimmt. Im Gegensatz dazu wirkt das orbitale Forcing, welches über Holozän-Zeitskalen dominiert, hauptsächlich auf die Nordhemisphäre. Deshalb kann man ein SEM mit Nordhemisphärentemperaturen antreiben und dadurch die Hauptkomponente der Meeresspiegeländerung über das Holozän simulieren. Es stellte sich heraus, dass eine zusätzliche konstante Rate, von der Größenordnung des antarktischen Beitrags zum Meeresspiegel, nötig ist, um den Meeresspiegelverlauf des Holozäns zu erklären. Der Meeresspiegel seit dem Holozän-Klimaoptimum kann also als eine Summe von temperaturbedingtem Fallen und einem langfristigen positiven Beitrag, wahrscheinlich einer andauernden Reaktion auf die Deglaziation der Antarktis, interpretiert werden.

Meeresspiegel, Klimawandel, Projektionen, Anthropogener Meeresspiegel, Holozän, Semiempirische Modelle

Contents

List of Figures

List of Tables

Chapter 1

Introduction

Approaching our planet one immediately recognizes it is blue. Oceans cover approximately 71% of Earth's surface and have a tremendous influence not only on the Earth and climate system, but also on human societies. These influences range over a very broad spectrum with one of them being sea level, the water level of the world's oceans. This, on first sight, simple concept in reality turns out to be quite a scientific challenge of great social importance.

1.1 Importance

Reconstructions from tide-gauge measurements, using different methods, found a 20th century linear rate of global sea-level rise of 1.3–1.9 mm/yr as shown in figure 1.2 (Hay *et al.* (2015), Church & White (2006), Church & White (2011), Jevrejeva *et al.* (2008), Ray & Douglas (2011), Wenzel & Schröter (2010), Wenzel & Schröter (2014)). Satellite altimetry measurements, which are available since 1993 (Nerem *et al.* (2010)), give a mean global rate of sea-level rise of 3.3 ± 0.4 mm/yr since then (see figure 1.2). A further increase in sea level and its rate of rise is to be expected over centuries (Schaeffer *et al.* (2012)) with impacts covering natural as well as human factors (IPCC (2013)). The physical impacts like submergence, salt-water intrusion in surface water and groundwater, increased flooding of coastal lands (Little *et al.* (2015), Storlazzi *et al.* (2015), Woodruff *et al.* (2013)) and increased erosion again have strong, direct and indirect, impacts on ecosystems and human societies (Roberts & Andrei (2015)). Impacted ecosystems are

for example salt marshes, coral reefs and mangroves (Nicholls & Cazenave (2010), Lovelock *et al.* (2015)). The societal impact can hardly be quantified by numbers but they give an impression: More than 600 million people live not higher than 10 meters above sea level. This accounts for 10% of the world's population on 2% of the world's land area (McGranahan *et al.* (2007)), with rapidly growing trends. Lichter *et al.* (2011) estimate 1–2.3% of the world's population living lower than 1 meter above sea level using three digital elevation models and two population datasets. Under a business-as-usual scenario of global greenhouse gas emissions Nicholls *et al.* (2011) estimated that 187 million people, which make 2.4% of the worlds population, are at risk of forced displacement by 2100. This is not only a threat to less developed countries or Small Island States (Storlazzi *et al.* (2015)), with coastlines hard to defend, but also cities like New York are endangered. Already now, due to sea-level rise, the mean flood heights in New York City increased by >1.2 meters from $\approx$ 850 to 2005 CE and a one-in-500-years flood now occurs every $\approx$ 24.4 years (Reed *et al.* (2015)). The mentioned consequences of sea-level rise and their projections to 2100 can be considered rather immediate because sea level is a distinctly slow responding part of the Earth system which makes a rise hard to stop. So by now we have already committed to sea-level rise over centuries to millennia. A paleodata estimate by Rohling *et al.* (2013) and Foster & Rohling (2013) finds a long-term sea-level commitment of likely >9 m with today's greenhouse-gas concentrations. Levermann *et al.* (2013) use a modelling approach to estimate long-term, multi-millennial sea-level commitment and find a medium rise of 10.9 meters for a two-degree warming above pre-industrial. The high inertia of sea-level rise, in addition to the mentioned severe consequences, make immediate action necessary.

1.2 What is sea level?

Given these numbers it is easily understood that sea-level change is often related to as a top-priority field in climate science (Church *et al.* (2011b)). At the same time it is a highly multi-disciplinary field of science. Sea level is here always referred to as a temporal (usually yearly) average to exclude

the effects of waves and tides. It is important to differentiate global-mean or eustatic sea level (GSL, figure 1.2), which is the focus of this work, from local or relative sea level (RSL). RSL is measured with tide-gauge stations and is the local difference between sea-surface and solid-earth height. Sea-surface height (or in IPCC (2013) terminology: geocentric sea level) again can be globally measured by satellite altimetry with respect to a reference ellipsoid (figure 1.1). GSL is understood as the volume of ocean water, uniformly distributed in the ocean basins, relative to a fixed reference frame. So either a change in volume of ocean water or the ocean basin can change GSL (IPCC (2007)). This can not be measured directly but can be calculated with different methods from tide-gauge and satellite measurements (figure 1.2). The earliest tide-gauge measurements started in 1700 CE in Amsterdam. Longer records can only be compiled with the inclusion of proxy data as done in chapter 5 (figure 5.3). RSL differs from the global mean due to a variety of factors, both climatic and non-climatic, which change the geoid height or result in vertical land motion as well as sea-surface height changes relative to the geoid. The climatic processes involve atmosphere-ocean dynamics while geological background processes include tectonics, sediment compaction and glacial-isostatic adjustment (GIA). Through the redistribution of ice and ocean masses so called "fingerprint" effects give rise to a distinct sea-level pattern. These redistributions result in geoid changes, vertical land motion and changes in the gravitational pull on ocean waters by, for example, ice sheets (Kopp *et al.* (2015)).

The ocean-water volume depends on its mass and density. The density is a function of temperature and salinity which cause the steric part of GSL change. The temperature-driven thermosteric change is about an order of magnitude bigger than the salinity-driven halosteric sea-level change. Therefore generally the main focus lies on the thermosteric part but both play an important role in certain regions with strong freshwater influx (Antonov (2002)). Mass changes are caused mainly by the melting of land-based ice from glaciers, ice caps and ice sheets. To a minor extent also human induced changes of landwater storage, in form of aquifer depletion and water retention in dams, play a role (Konikow (2011); Chao *et al.* (2008)). The sum of all these effects forms the sea-level budget which could first be closed,

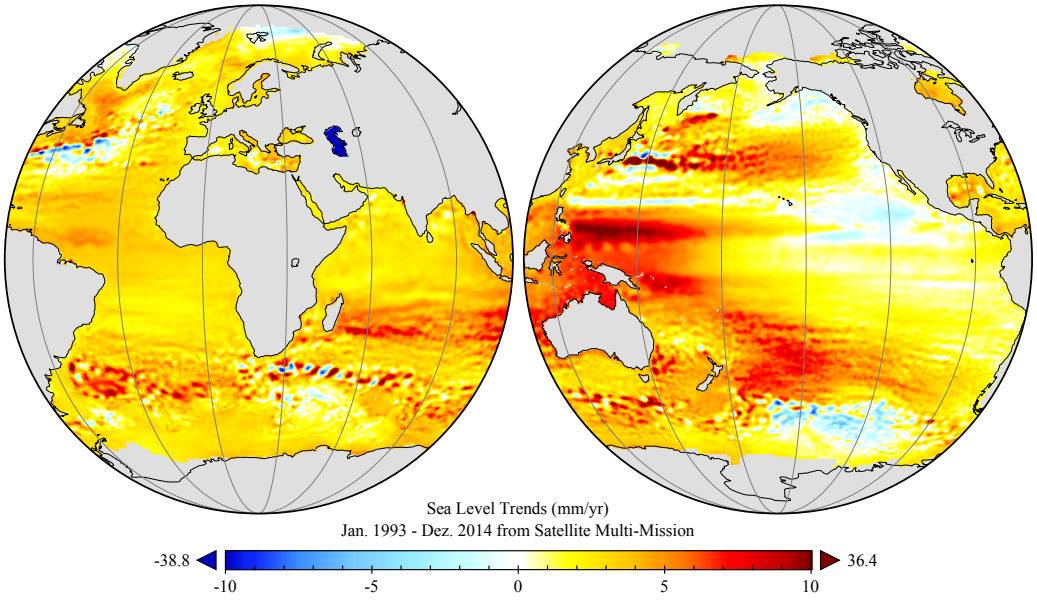

Figure 1.1: **Sea-level trends 1993–2014 CE.** Mean sea-level trends (mm/yr) from a combination of satellite data (Nerem *et al.* (2010)).

within uncertainties, in Church *et al.* (2011a) for the period 1972–2008 CE. For this period a combination of models and data is needed. Only since 1993 the budget can be determined purely by observations, with thermal expansion and glacier melting (excluding Greenland and Antarctica) being the two largest terms, accounting for 35 and 25% respectively (IPCC (2013)). The IPCC's 4th Assessment Report (IPCC (2007)) still underestimated the sum of all GSL contributions which illustrates the complexity of the problem and one big advancement made since then (IPCC (2013)).

1.3 Modelling sea level

In order to model global or local sea level from first principles, coupled models for most components, contributing to GSL change, would be necessary. Components with minor feedbacks like glaciers (excluding the ice sheets) and land-water storage might suitably also be modelled offline. Usually, coupled Atmosphere-Ocean General Circulation Models (AOGCM) only model thermosteric sea-level change (IPCC (2013)). For modelling the contribution from glaciers and ice caps calibrated mass-balance models are commonly used, driven with temperature- and sometimes precipitation-output

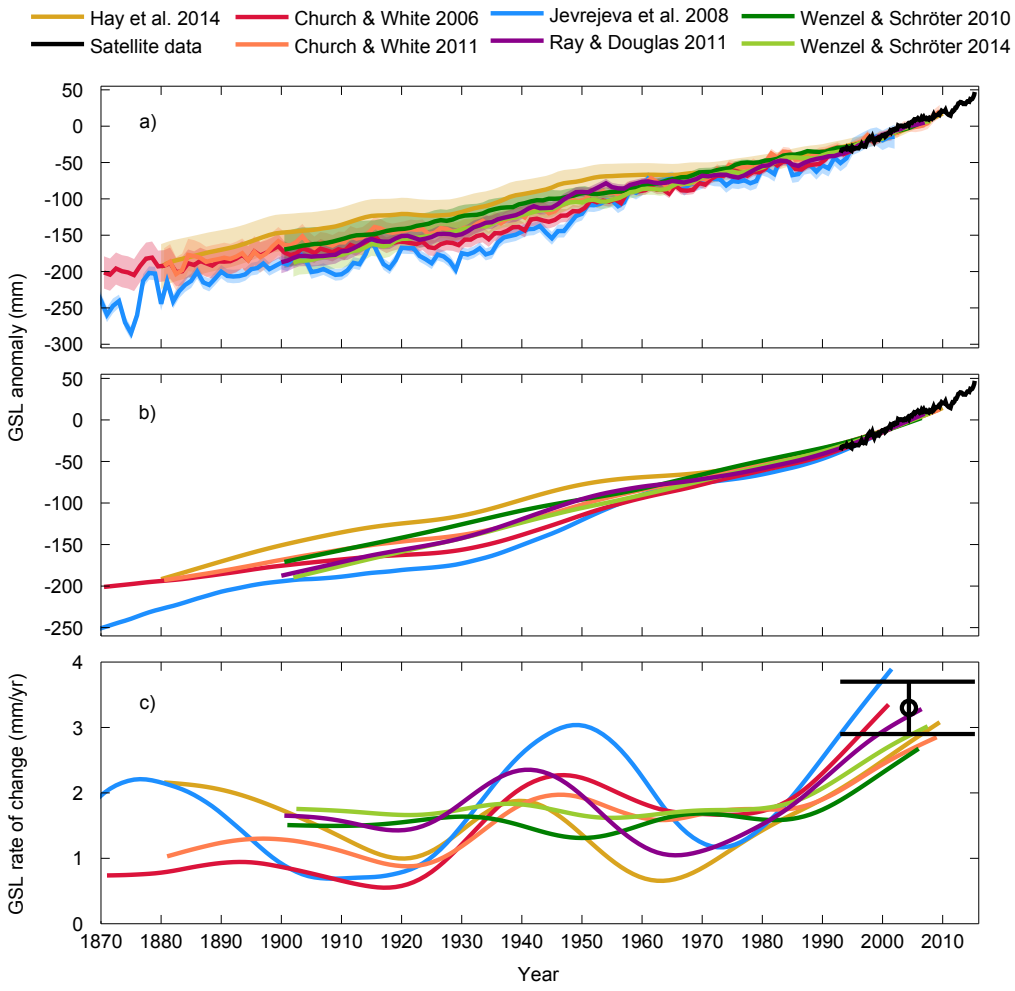

Figure 1.2: **Different global sea-level (GSL) reconstructions from literature.** (a) Comparison of different global sea-level reconstructions with one standard deviation. (b) Same as (a) but ssa smoothed (Moore *et al.* (2005)) with a 30-year filter width and without uncertainty for easier comparison. (c) The rates of sea-level rise calculated from the smoothed GSL curves of panel (b). The rates themselves are ssa smoothed with a filter width of 30 years. The comparably short satellite measurements are given as a range only. The colours correspond to: yellow - Hay *et al.* (2015), black - Nerem *et al.* (2010) (Satellite data downloaded at the 16th of September 2015), red - Church & White (2006), orange - Church & White (2011), blue - Jevrejeva *et al.* (2008), purple - Ray & Douglas (2011), dark green - Wenzel & Schröter (2010), light green - Wenzel & Schröter (2014)

from GCMs (Radić & Hock (2011), IPCC (2013)). The ice-sheet component of GSL, which is potentially very important, given the amount of ice stored in Greenland and Antarctica, is the least understood. For the IPCC (2007) AR4 ice-sheet contributions were estimated with the mass balance sensitivity of Gregory & Huybrechts (2006). To accommodate a possible additional contribution by ice discharge, a constant rate, based on observations, was added. Finally, the possibility of dynamic effects was accounted for by an additional contribution without firm theoretical or observational basis (Church *et al.* (2011b)). From AR4 to AR5, models as well as scientific understanding improved (Winkelmann *et al.* (2012); Alley & Joughin (2012); Nick *et al.* (2013); Mengel & Levermann (2014)) and observations give a clearer picture of the ice-sheets mass balances (Chen *et al.* (2013), Rye *et al.* (2014)). Still, the projections of sea-level contributions from Antarctica hardly show any dependence on the greenhouse-gas scenario used. Ice-sheet dynamical changes are assumed to be scenario independent because of the lack of knowledge to quantitatively assess this contribution (IPCC (2013)).

Clearly, modelling GSL (not to speak of RSL) with process-based models is a complicated task because of the variety of interwoven processes. Willis & Church (2012) summarize some of the problems these models are facing which include most of the involved components, namely uncertainties in deep ocean heat uptake and expansion, snowfall on Antarctica, ocean circulation underneath ice shelves and glacier and ice-sheet response. The model shortcoming can furthermore be investigated by comparisons with measurements as done by Rahmstorf *et al.* (2007) and Rahmstorf *et al.* (2012). Rahmstorf *et al.* (2012) show that best GSL estimates as modelled in the IPCC (2007) AR4 are 60 and 50% lower than observations for the periods 1993–2011 and 1961–2003 CE (see also chapter 2.4). This model shortcoming also has strong implications for 21st century projections which were unrealistically low in the IPCC (2007). As Rahmstorf (2010) points out, the projected best estimate of 35 cm GSL rise by the 2090s, compared to 1990, implies no GSL acceleration beyond present level despite $\approx 3^{\circ}$C warming for the A1B scenario (IPCC (2000)). Given that the rate of GSL rise approximately tripled over the 20th century in response to only 0.8°C warming, these projections seem to underestimate the future rise dramatically. While

the lower bound of the IPCC projections changed only slightly from the first (FAR, IPCC (1990)) to the fourth Assessment Report (AR4, IPCC (2007)), the upper bound, and thus the total uncertainty, dropped drastically. Only the AR5 (IPCC (2013)) increased projections considerably as summarized for high emission scenarios in figure 1 of Jevrejeva *et al.* (2014). This is mainly due to the inclusion of rapid changes in ice-sheet outflow, improved Greenland-surface mass-balance models and a higher glacier contribution on the grounds of higher estimates of the global glacier volume (IPCC (2013)). Results published since the AR5 (IPCC (2013)) all fall within its likely ranges (Clark *et al.* (2015)) but still, the projections have clear shortcomings like the scenario independency of the Antarctic sea-level contribution.

1.4 Semi-empirical alternatives

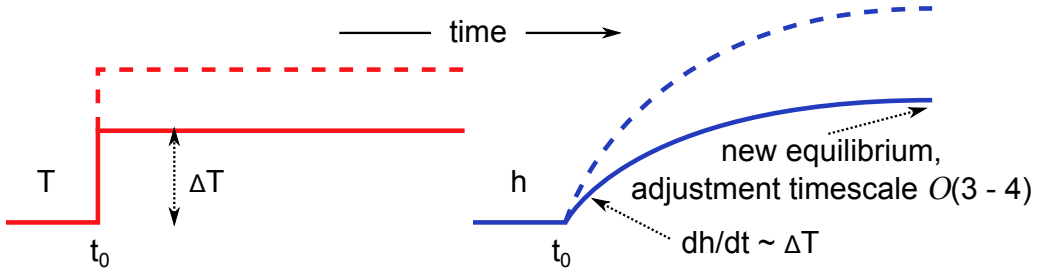

Figure 1.3: **Sea-level response to temperature change.** Schematic response of sea level (h) to step-like changes in temperature (T) at time t_0 (after Rahmstorf (2007)). Two examples of different magnitude are shown in solid and dashed lines.

Semi-empirical models (SEMs) are an alternative to process-based models, which in many respects fail due to excessive complexity. Semi-empirical models exploit physics-based empirical relationships of sea level to some forcing. Already Gornitz *et al.* (1982) fitted a linear relation, via least-square regression, between global mean surface temperature (T) and global sea level (h) of the form $h(t) = aT(t - t_0) + b$. The record lengths of temperature and sea level were too short for robust assessments, but interestingly they found a time lag (t_0) of 18 years which is of the order of magnitude of the typical response time of thermal expansion. In the light of the unre-

alistically low IPCC GSL projections, Rahmstorf (2007) introduced a semi-empirical approach to model sea level which was widely acknowledged and discussed. Subsequently, different semi-empirical model formulations were published and used by a multitude of groups; only to mention some publications: Vermeer & Rahmstorf (2009), Jevrejeva & Moore (2009), Grinsted *et al.* (2009), Rahmstorf *et al.* (2011), Kemp *et al.* (2011), Schaeffer *et al.* (2012), Bittermann *et al.* (2013), Orlić & Pasarić (2013). The basic idea was outlined by Rahmstorf (2007) and is schematically shown in figure 1.3. Global sea level is expected to rise in response to an increase in global temperature. Depending on the response time, which is of the order of centuries to millennia, GSL will asymptotically approach a new equilibrium if temperature stays constant for long enough. PALSEA (2010) investigated patterns of temperature-forced sea-level change during the termination of the last glacial and proposed three possible general patterns: (i) exponentially increasing, (ii) linear or (iii) asymptotic. An exponential increase to a step-like temperature change could be excluded by paleo-data constraints. A linear or asymptotic (figure 1.3) behaviour were found to be possible, the latter one was proposed by Rahmstorf (2007). But even if the full response of sea level might be unknown, the first response, lasting maybe a few centuries, can be approximated as linear. This results in the model equation 1.1 where the rate of GSL rise $\mathrm{d}h/\mathrm{d}t$ equals the deviation of global near-surface air-temperature T from an equilibrium temperature T_0 times the sea-level sensitivity a:

$$\mathrm{d}h(t)/\mathrm{d}t = a\,(T\,(t) - T_0) \tag{1.1}$$

Refined versions of equation 1.1 were published by Vermeer & Rahmstorf (2009) (equation 1.2), Kemp *et al.* (2011) (equation 1.3) and in chapter 5. Vermeer & Rahmstorf (2009) add a rapid response term $b\ \mathrm{d}T/\mathrm{d}t$ which significantly improves simulations because it better captures fast processes like heat uptake in the ocean's mixed layer:

$$\mathrm{d}h(t)/\mathrm{d}t = a\,(T\,(t) - T_0) + b\ \mathrm{d}T(t)/\mathrm{d}t \tag{1.2}$$

Kemp *et al.* (2011), for the first time, semi-empirically modelled GSL for the past millennium with the model equations 1.3. For these ends, it was nec-

essary to introduce a relaxation time scale τ during which the equilibrium temperature T_0 decays to the actual temperature T. This way a new equilibrium sea level can be reached:

$$\begin{aligned} \mathrm{d}h(t)/\mathrm{d}t &= a_1 \left(T\left(t\right) - T_{00}\right) + a_2 \left(T\left(t\right) - T_0\left(t\right)\right), \\ \text{with } \mathrm{d}T_0(t)/\mathrm{d}t &= \left(T\left(t\right) - T_0\left(t\right)\right)/\tau. \end{aligned} \tag{1.3}$$

Other groups use global mean radiative forcing as drivers for their models (Jevrejeva & Moore (2009)) and different model formulations but following the same principles described above.

In spite of being a pragmatic and by now well tested approach to GSL modelling, semi-empirical models, no matter of which form, have clear limitations. They are motivated by basic physics, but at the same time they are a simplistic approximation of complex, not yet fully understood processes on very different time scales. Being calibrated to past data the assumption is necessary that the sum of processes, governing GSL, behave unchanged in future. If, for example, ice sheets start to lose mass in a non-linear fashion because of positive ice-flow feedbacks, as some observations already imply (Joughin *et al.* (2014)), semi-empirical models are not able to capture this and can thus only give lower projection limits. On the other hand, it was argued that components important during the calibration period could play a minor role in future, in which case semi-empirical models would overestimate GSL change. One potential candidate for this would be glaciers and ice caps that might disappear during the course of the 21st century. However, first of all this is rather unlikely in the near future, given the global glacier volume ($\approx$ 40 cm mean sea-level equivalent, excluding Antarctica and Greenland, IPCC (2013)) and secondly semi-empirical models do not distinguish between glaciers and ice sheets. As explained in Rahmstorf (2010) and Rahmstorf *et al.* (2011), the melting of ice depends on the local temperature and with increasing temperatures more ice can be melted in regions were it was previously stable. Even if all glaciers would disappear, there would be plenty of ice to melt from ice sheets. Still, it is not clear whether semi-empirical projections rather over- or underestimate GSL. But clearly GSL projections by SEMs have been systematically higher than those

of process-based models. This can be seen in figure 13.12 and summary table 13.6 of IPCC (2013). Rahmstorf *et al.* (2011) explored in detail the robustness of different model assumptions and in chapter 2 the predictive capability of semi-empirical models is tested. Results still need to be taken with caution, but up to now, semi-empirical models could not be falsified and proved to be a good supplement to process-based models to explore the uncertainties in GSL projections.

1.5 Thesis outline

In the following, SEMs will be looked at from different perspectives. As already mentioned, chapter 2 is dedicated to testing the predictive skills of SEMs by predicting historical sea level not included in the calibration period.

Following the idea that GSL should be the sum of its components $h = \sum h_i$, chapter 3 attempts to simulate the glacier and ice-cap component. Vermeer & Rahmstorf (2009) could already show that thermal expansion can be modelled satisfactorily with SEMs, so the second biggest historical contribution to GSL is an interesting target but the data availability is far worse.

Kemp *et al.* (2011) were confronted with a problem while calibrating their model over the last 1.5 millennia: A $\approx$ 0.2°C temperature step around 1100 CE, in the data of Mann *et al.* (2008), turned out to be incompatible with the sea-level record. This problem is investigated in chapter 4 where a better error representation as well as a different temperature data set both indicate that the problematic temperature step might be an artefact of the data.

Yet a truly global sea-level data set was not available for pre-industrial periods. A compilation like this is presented in chapter 5. With this newly compiled GSL, new 21st century projections are presented which seem to close the gap between SEMs and process-based models. Although this might be purely coincidental, it can be regarded a big step because now evidence from very different models give very similar projections, making those more reliable. Additionally the anthropogenic part of today's GSL rise is calculated, showing that indeed most of the present day rise is caused by global warming.

Finally the view is broadened in chapter 6, attempting to model GSL over

the whole Holocene from about 10,000 BCE (Before the Common Era) to 1800 CE. This is achieved in spite of a rising GSL with simultaneously sinking temperature from the Holocene climatic optimum onward. The main messages from this last chapter are the time-scales on which sea-level relaxes and the need of an additional constant rate which can possibly be related to the long time-scale response of Antarctica.

Chapter 2

Validating semi-empirical models

The foundation for this chapter is the study Bittermann *et al.* (2013), which uses the same figures, tables and parts of the text.

Besides the ability to reproduce past data not used in constructing the model, a major ingredient for any physical model is its predictive skill. For semi-empirical models, which are calibrated against data to make projections, it is additionally important to analyse their predictive skill beyond the ranges of the calibration period. For sea-level projections this last point is of high importance because even the lowest, physically sensible projections for the 21st century are beyond the range of pre-industrial or even today's sea-level. In the following semi-empirical models are calibrated against parts of the data to then forecast the rest of the data. For such forecasts, at the time of this study, two sea-level data sets were available and long enough to be suited for calibrating the semi-empirical models: the tide-gauge data set of Jevrejeva *et al.* (2008) covering the period 1700–2002 CE (henceforth JE08) and the proxy data set of Kemp *et al.* (2011) covering -100–2000 CE (henceforth KE11). The proxy data are from one location only, but as discussed in detail in Kemp *et al.* (2011), they are expected to represent the global sea-level (GSL) evolution to within $\pm$ 10 cm, and thus still provide a useful calibration target due to the long time period covered. For global-mean temperature over land and ocean, the long proxy data set from Mann *et al.* (2008) covering 500–2006 CE was used. The best results are obtained when constraining the semi-empirical model using a combination of tide-gauge and proxy data. However, as intermediate steps to study the sensitivity of

the approach, the model performance using either only tide-gauge or only proxy data is shown. Finally a comparison to the IPCC (2007) AR4 sea-level forecast of the period 1961–2003 is done. Therefore also the Church & White (2011) (CW11) GSL compilation is used as calibration target.

2.1 Calibration on tide-gauge data

Before using GSL data compiled from tide gauges as input for climate driven models it is advisable to remove non-climatic factors like reservoir storage (Chao *et al.* (2008)) and groundwater extraction (Konikow (2011)), although the effects on GSL are small. Removing these two factors leads to a change in sea level by less 2 cm, 30 mm by reservoir storage (Chao *et al.* (2008)) and -13 mm by groundwater extraction (Konikow (2011)). For more details see Rahmstorf *et al.* (2011). The semi-empirical sea-level model for calibrations on the JE08 tide-gauge data is given by equation 1.2. The methods followed were those described in Rahmstorf *et al.* (2011). The integration constant H_0, i.e. the vertical offset of the modelled sea level to the JE08 sea level, was chosen so that the means over the period 1700–1800 CE of both match. The end of the calibration period was then restricted to times ranging from 1860 to 1960 and the sea-level development up to the present was projected.

The figures 2.1 and 2.2 summarize the results. As suspected calibrations get better with longer calibration periods which is reflected in the parameter convergence shown in figure 2.2. While a calibration until 1860 fails to sufficiently constrain the model, useful projections are obtained with calibrations up to 1880 or later. For all calibrations shown in figure 2.1 the uncertainties of the semi-empirical model and the JE08 data overlap although only just for calibrations until 1940 and 1960. Except for the calibration until 1860 the model systematically overpredicts sea-level rise by 11–70%. This might well be due to the steep increase in the JE08 data until 1960, compared to later, which is not found to the same degree in other GSL data compilations (see figure 1.2).

When calibrated to the period 1700–1900 CE, the model predicts a 20th century sea-level rise ranging from 5 to 41 cm (90% confidence) with a best

estimate of 23 cm (figure 2.1), while the observed linear 20th century rise in the JE08 data (with landwater adjustment) is 16 to 26 cm (table 2.1). Despite its large uncertainty, the best estimate of the prediction lies well within the observational range although the sea level during the calibration period varies only little. The model even correctly predicts the period of flat sea level from 1900 to 1930 CE and the subsequent decades of steep rise; only after 1970 does it start to deviate a few centimetres from the tide-gauge data.

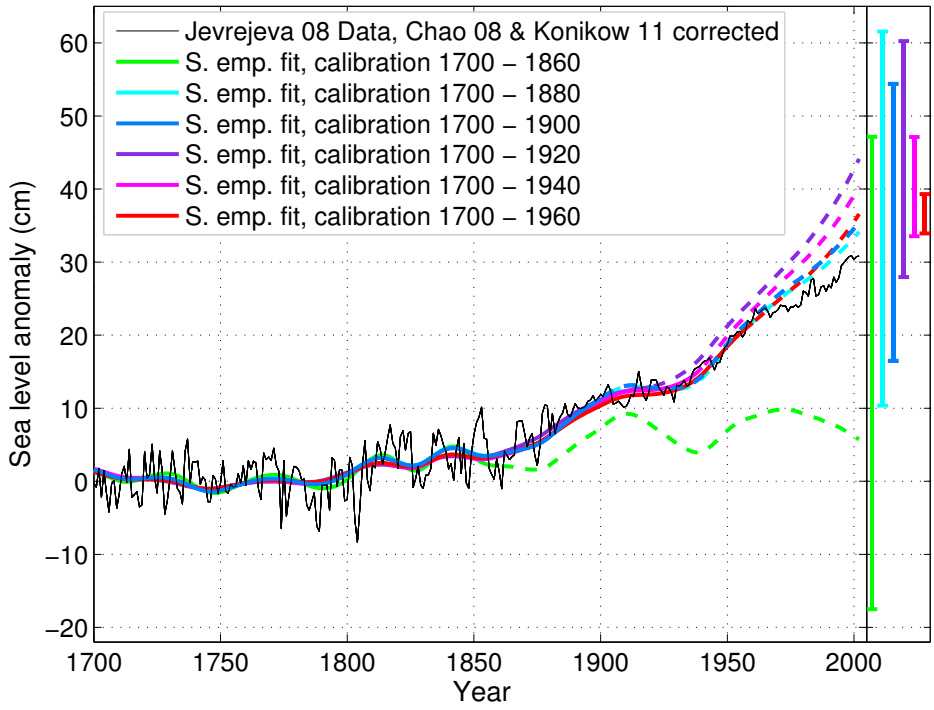

Figure 2.1: **Sea-level forecasts based on the GSL data of Jevrejeva *et al.* (2008) (JE08).** The different colours denote different calibration periods of the model (1700 to 1860, 1880,...,1960 CE). Solid lines show the calibration period while dashed lines give the forecasts. The bars on the right hand side give the 90% confidence of the forecasts, starting from the last year of calibration onwards.The parameter a was constrained to be $\geqslant 0$. The JE08 data used for calibration, was adjusted for ground water pumping (Konikow (2011)) and reservoir storage (Chao *et al.* (2008)).

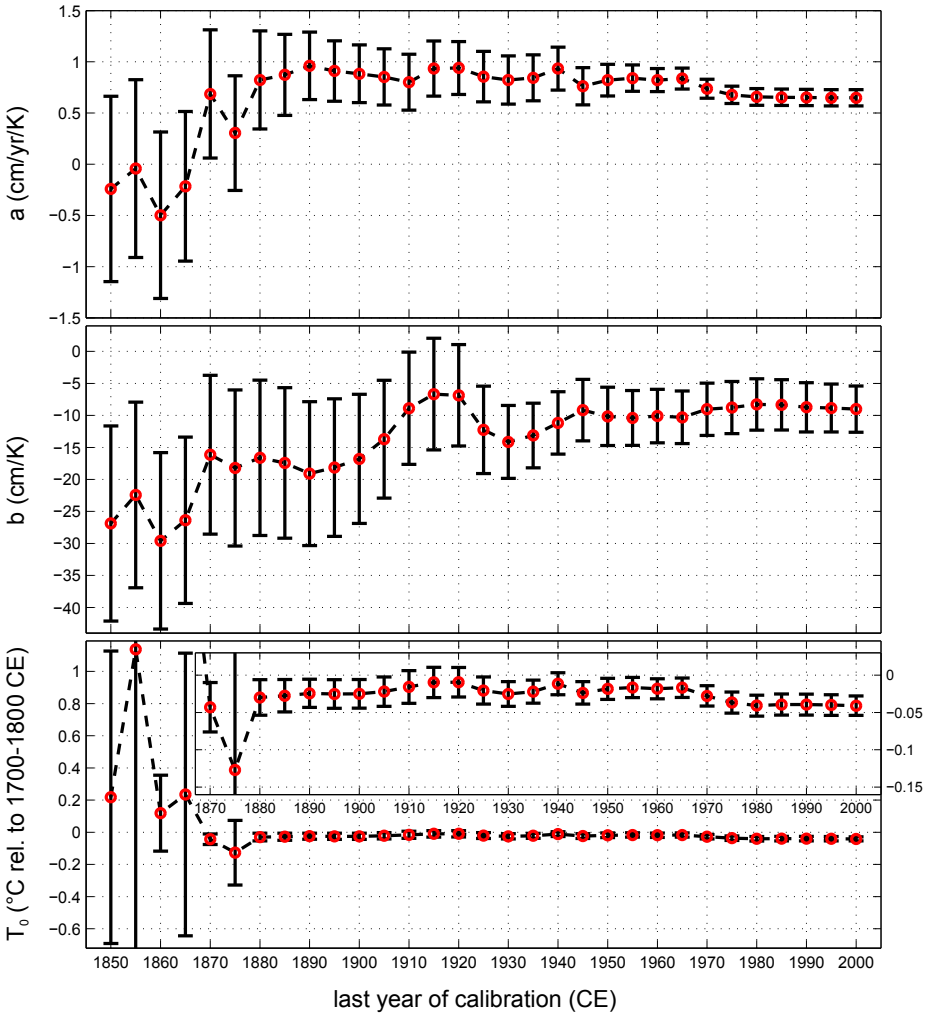

Figure 2.2: **Parameter dependency on calibration period.** The parameters a, b and T_0 from equation 1.2 with $1\ \sigma$ uncertainty shown against the last year of calibration on the JE08 data, starting 1700 CE. The inset in the lower panel zooms in on the vertical scale.

2.2 Calibration on proxy data

Two major differences of proxy compared to tide-gauge data are record length and time resolution. As discussed earlier, this makes a few adjustments to the semi-empirical model necessary. The formulation used for this study is given in equation 1.3. For the semi-empirical model calibrated with proxy data the fast response term of equation 1.2 is dropped. The term reflects the ocean mixed layer response (Vermeer & Rahmstorf (2009)) on a time scale not resolved by the proxy data. On the other hand the temperature driven part of the equation is split in two, one 'perpetual' part and one decaying on an explicit timescale τ. This second part allows the model to find a new equilibrium on the multi-centennial timescale τ while the 'perpetual' part covers effects like glacial isostatic adjustment or ice-sheet responses which act on multi-millennial timescales, exceeding the data coverage. For more details on the Monte Carlo method applied see the methods subsection 2.6.

Following previous publications (Kemp *et al.* (2011), Rahmstorf *et al.* (2011) and Schaeffer *et al.* (2012)) data before 1000 CE is discarded for calibration because the relatively warm Mann *et al.* (2008) data was found not to be consistent with the stable sea-level reconstruction of Kemp *et al.* (2011). See also chapter 4 for a more detailed look on this issue.

As shown in figure 2.3 all calibrations up to 1900 CE or earlier give about the same, underestimated projection. For the calibration up to 1900 CE the projected 20th century rise is 5–18 cm with 90% confidence which overlaps with the observed GSL range from tide gauges of 14–26 cm (table 2.1). One reason for this underestimation could be the broad, uninformative, prior distributions used for the model parameters (table 2.3). On the other hand these work well if calibrating the model until 2000 CE. So the underestimation might rather be due to the low time resolution of the proxy data which does not well resolve sea level between 1860–1900 CE which provided a calibration target for the JE08 data before. Consequently it makes sense to combine both proxy and tide-gauge data to take advantage of the long time coverage and long period of stable sea level, which is useful for constraining T_0, as well as the high time resolution in the last centuries.

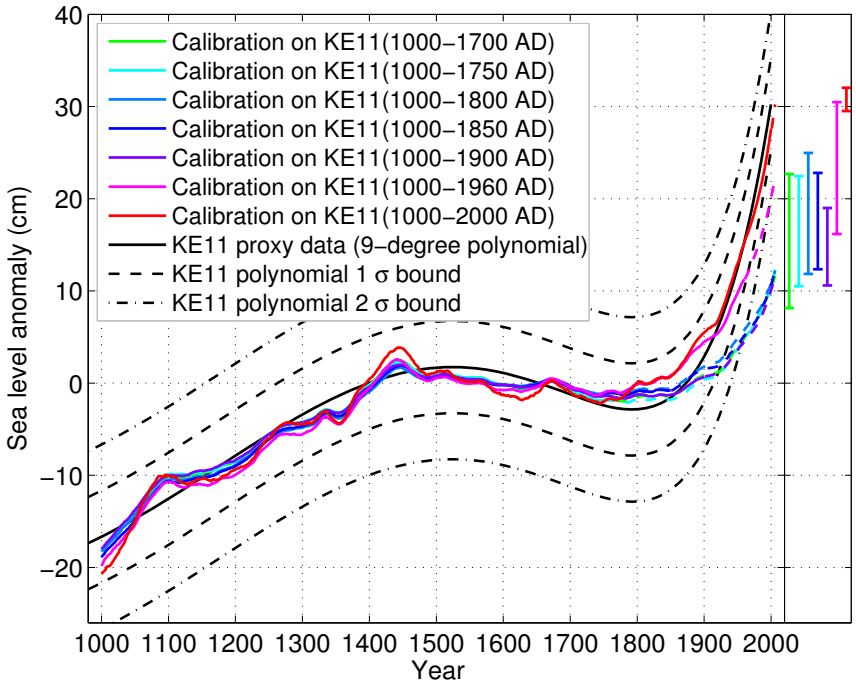

Figure 2.3: **Sea-level projections based on the proxy data of Kemp *et al.* (2011) (KE11).** Experiments with varying calibration periods are marked with different colours. The sea-level anomaly is given relative to the period 1400-1800 CE. The solid, coloured lines represent the calibration period, the dashed lines show the projection from the end of the calibration period until 2006. The bars on the right give the 90% confidence level of the projections. In black a 9-degree polynomial fitted to the KE11 data with 1 σ and 2 σ confidence interval is shown.

2.3 Calibration on combined tide-gauge & proxy data

As mentioned above it brings advantages to use proxy and tide-gauge data in combination. This is also what had been done in previous simulation work (Kemp *et al.* (2011), Rahmstorf *et al.* (2011), Schaeffer *et al.* (2012)) where the prior distributions of the parameters had been constrained with tide-gauge data. So now the KE11 proxy data is used up to 1700 CE and from there on until 1900 CE the JE08 data. Both data have been combined by aligning them over their period of overlap.

The results are summarized in figure 2.4 and table 2.1. The dashed blue line with grey uncertainties in figure 2.4 shows the 20th century projection of the semi-empirical model if calibrated only up to 1900 CE. It is in very good agreement with the green JE08 data (table 2.1) although the forecasted rates are about three times higher than during the calibration period. As mentioned above this is very important because future rates are expected to exceed current rates about the same way.

Table 2.1: **Comparison of the rates of sea-level rise 1901–2000 CE.** Proxy (KE11, Kemp *et al.* (2011)) and tide-gauge (JE08, Jevrejeva *et al.* (2008)) data sets have been used for the semi-empirical forecasts as described in the text (see figures 2.1 and 2.3). The abbreviation KE11 & JE08 denotes the merged data set from figure 2.4. The rates are calculated as linear trends.

	Data Source	Calib. Period CE	Rate mm/yr 50 %	5–95 %
SEM fit	KE11 & JE08	1000–1900	2	[1.3–3.0]
	KE11	1000–1900	1	[0.5–1.8]
	JE08	1700–1900	2.5	[0.9–4.1]
Data	JE08	X	2.1	[1.6–2.6]
	CW11	X	1.7	[1.4–2.1]

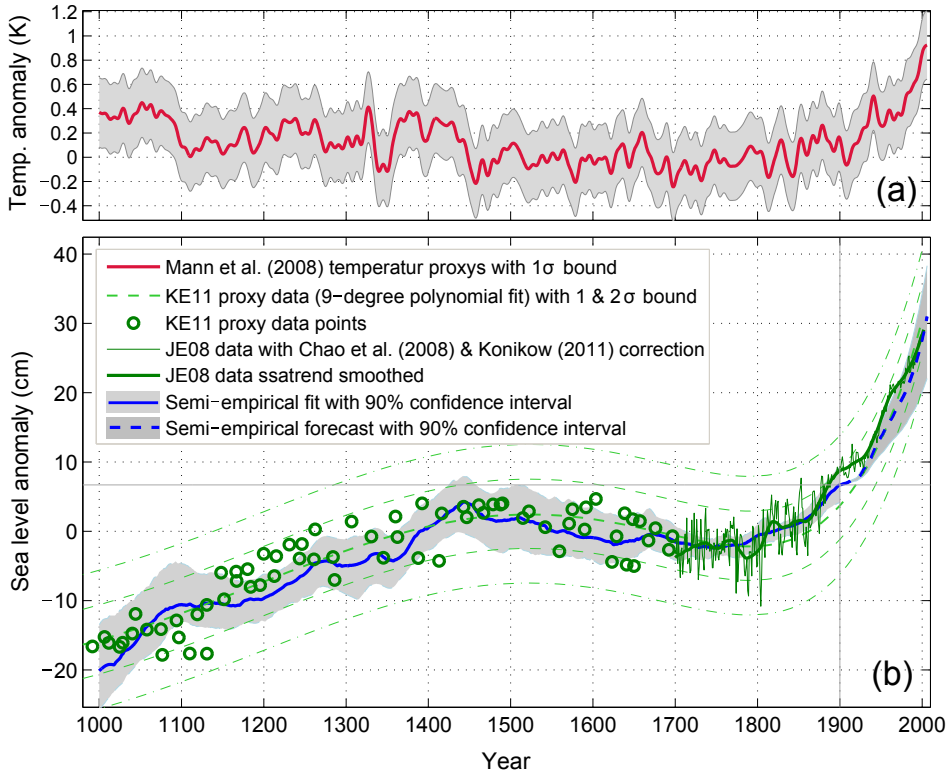

Figure 2.4: **Semi-empirical 20th century forecast with combined proxy and tide-gauge data.** (a) Mann *et al.* (2008) temperature proxy data with 1 σ error used for calibration and forecasting. (b) Semi-empirical fit to a combination of proxy (Kemp *et al.* (2011)) and tide-gauge data (Jevrejeva *et al.* (2008)). The semi-empirical calibration is shown as a solid blue line with grey 90% confidence. The dashed blue line gives the forecast for the last century, again with 90% confidence. Overlaid the data points of the KE11 proxies until 1700 as well as a 9-degree polynomial fit to the full set of KE11 proxies with 1 and 2 σ uncertainty are shown. Plotted in green from 1700 CE onwards is the JE08 tide-gauge data and for the sake of clarity a ssa-smoothed version with a filter width of 30 years. The GSL from tide gauges are corrected for reservoir storage (Chao *et al.* (2008)) and ground water pumping (Konikow (2011)).

2.4 Comparison with IPCC AR4 forecasts

Since this study was conducted during the preparation of the IPCC (2013) AR5 it was especially interesting to compare the IPCC (2007) AR4 forecasts to the capabilities of semi-empirical models. For these ends the models were calibrated up to 1960 CE to forecast sea level from there up to 2003. In addition to the JE08 and KE11 data, which were used as before a third set from Church & White (2011) (CW11) was used, starting in 1880. The CW11 data was used in combination with the GISS (Goddard Institute for Space Studies) temperature (Hansen *et al.* (2010a)).

Table 2.2 shows the calculated rates, compared to data as well as the IPCC (2007) AR4 forecasts. It is important to note that the so called 'model-based' AR4 sea-level estimates did include ice-sheet contributions from observation (+0.19 [-0.24–0.62] mm/yr) not simulation. Otherwise the given rate would probably have been even lower because the models used for the AR4 showed negative ice-sheet responses, i.e. an accumulation instead of a loss of water (Van den Broeke *et al.* (2011), Rignot *et al.* (2011) & Alley & Joughin (2012)).

Calibrations to the KE11 and CW11 sea level give an excellent 43 year forecasts when compared to the data while the JE08 calibration overpredicts the rise. This overprediction is not due to the longer time coverage as compared to CW11 but to the strong increase of sea level right up to the end of the calibration period in 1960 which is not found to this degree in other data (see figure 1.2). These differences arise because CW11 use a more advanced sampling method as compared to JE08 and can thus deal better with spatial under-sampling of tide-gauge stations (Rahmstorf *et al.* (2011)). It is thus reasonable to put more trust in the CW11 calibration as compared to JE08. Despite the added ice-sheet contributions from observations, IPCC (2007) AR4 model-based estimates underestimate sea-level rise since 1960, with 90% confidence intervals only hardly overlapping, which is also acknowledged by the IPCC.

Table 2.2: **Comparison of the rates of sea-level rise 1961–2003 CE.** Proxy (KE11, Kemp *et al.* (2011)) and instrumental (JE08, Jevrejeva *et al.* (2008) as well as CW11, Church & White (2011)) data sets have been used for the semi-empirical forecasts as described in the text (see figures 2.1 and 2.3). The rates are calculated as linear trends. The AR4 forecast can be found in IPCC (2007), table 9.2.

	Data Source	Calib. Period CE	Rate mm/yr 50 %	5–95 %
SEM fit	KE11	1000–1960	2.1	[0.8–4.1]
	JE08	1700–1960	3.5	[2.8–4.1]
	CW11	1880–1960	2.0	[1.9–2.3]
IPCC	"ALL"	X	1.2	[0.7–1.7]
Data	JE08	X	2.0	[1.2–2.9]
	CW11	X	2.2	[1.7–2.6]

2.5 Conclusions

In this chapter it could be demonstrated that previously published semi-empirical models have good predictive skills even for rates well outside those of the calibration period. The exact quality of the projections depends on the data used and the reference data to compare it with. Using a combination of tide-gauge and proxy sea-level data for calibration, a 20th century sea-level rise of 13–30 cm (90% confidence range) is predicted while the observed interval from two tide-gauge based GSL data sets is 14–26 cm. When comparing predictive skills from 1961–2003 CE for different calibration data, excellent predictions are achieved with Kemp *et al.* (2011) and Church & White (2011) data while sea level gets overestimated when using the data of Jevrejeva *et al.* (2008). This overestimation is owed to a strong increase of sea level, in the data of Jevrejeva *et al.* (2008), right up to the end of the calibration period in 1960, which is not found to this degree in other data (see figure 1.2).

Challenged by these results Church *et al.* (2013) made an effort to show the predictive skill of the new IPCC (2013) AR5 models and directly compared them to the above results. They could show that the projections im-

proved but still lay at the lower end of the uncertainty interval of the observed sea level.

2.6 Methods

The Bayesian formalism for the analysis of the proxy (KE11) and the merged proxy tide-gauge (KE11 & JE08) data set was used the following way (Kemp *et al.* (2011), Schaeffer *et al.* (2012)):

$$P(\theta|x) = \frac{P(x|\theta)}{P(x)} P(\theta) = \mathcal{L}_x(\theta)\ P(\theta) \tag{2.1}$$

$$\mathcal{L}_x(\theta) = \exp\left(-\frac{1}{2}\, r'\, \Sigma^{-1}\, r\right) \tag{2.2}$$

$$\text{and } \theta = \left[a_1, a_2, b, \tau, H_0, \langle\tilde{T}_0\rangle, T_0(1000), T(t)\right] \tag{2.3}$$

Where $P(\theta)$ are the prior probabilities for the parameters θ and $\mathcal{L}_x$ denotes the likelihood distribution for the calculated sea level depending on the covariance matrix of the observations Σ and the residuals of data and simulation r. As shown in table 2.3 broader and uniform a priori distributions on the parameters θ, listed in table S3 of the supporting information of Kemp *et al.* (2011), were applied. The parameter b, controlling short term variations in sea level which are not resolved in our data, is superfluous and was dropped.

The integration constant H_0 accounting for the vertical offset was chosen so that the data and the fit match over the period of relatively constant sea level 1400–1800 CE in contrast to previous studies where H_0 was considered a model parameter. A sensitivity test showed indeed that the difference in forecast and error for different H_0 priors is only small. So is the difference of simulations with different a priori τ distributions as long as $\tau \neq \infty$.

For the analysis of the proxy data the covariance matrix Σ is taken to be a diagonal matrix consisting of the observational errors since the covariance structure is unknown. When analysing the merged KE11 & JE08 data set we use the diagonal matrix for the KE11 part of the data until 1700 CE and from there on the covariance matrix reported in Grinsted *et al.* (2009).

Table 2.3: **The a-priori distributions $P(\theta)$ for the Bayes update of equation 1.3.** The distributions of the temperature and τ are chosen as given in the supplementary table S3 of Kemp *et al.* (2011). $U[\alpha, \beta]$ denotes a uniform distribution between α and β, $U_{Sum}[\alpha_{sum}, \beta_{sum}]$ is the pyramid shaped sum of two uniform distributions U_1 and U_2 with $\alpha_{sum} = \alpha_1 + \alpha_2$ and $\beta_{sum} = \beta_1 + \beta_2$. The brackets $\langle\rangle$ stand for the mean over the given period.

Parameter	Prior Distribution
a_1	$U[0,1]$ cm/yr/K
a_2	$U[0,1]$ cm/yr/K
$a = a_1 + a_2$	$U_{sum}[0,2]$ cm/yr/K
b	0
$\langle \tilde{T}_0\,(recent)\rangle$	$\langle T\,(1400-1800\ \text{CE})\rangle\ +\ U[-0.3, 0.3]$ K
$T_0\,(1000\ \text{CE})$	$\langle T\,(1000-1100\ \text{CE})\rangle\ +\ U[-0.3, 0.3]$ K
τ	$400 * \exp(U[-2,2])$ yrs

Chapter 3

Semi-empirical modelling of glacier contributions to GSL

In this chapter a single component of contemporary sea-level rise, namely glacier and ice cap (GIC) melting, will be modelled semi-empirically. The foundation for this study is the data set of Radić & Hock (2011). It will turn out that this data does not allow a consistent semi-empirical calibration. Nonetheless the semi-empirical model helps to point out possible flaws in the underlying data.

The semi-empirical sea-level model (equation 1.1) introduced by Rahmstorf (2007) (RT) was formulated to simulate global mean sea level, which it did remarkably well. Later, Vermeer & Rahmstorf (2009) (VR) were able to show that also a single component of sea level, namely the thermal expansion, could be modelled semi empirically. For these ends they used climate model data, which only captured thermal expansion, and introduced a rapid response term $b\ \mathrm{d}T/\mathrm{d}t$ to their model equation 1.2. This rapid response term could account for the rapid heat uptake of the ocean's mixed layer, causing a sea-level rise of $\Delta h = d\ \alpha\ \Delta T = b\ \Delta T$ where d denotes the mixed layer depth and α the thermal expansion coefficient. Applying a typical value for $\alpha = 2.5 \times 10^{-4} K^{-1}$ and the rapid response term b from the calibrated model they could calculate a mixed layer depth of $d = 100$ meter which is a physically plausible value, giving additional trust in the method.

The IPCC (2013) AR5 estimated that in recent years (1993–2010 CE) the contribution of thermal expansion to global sea-level rise was the highest

with 35%, followed by glacier mass loss with further 25% (not including glaciers from Greenland and Antarctica). For longer periods the contributions are much harder to evaluate but together both effects contributed about 75% of global sea-level rise from 1971–2010 CE. Glacier melt and its subsequent contribution to global sea-level rise not only accelerated over past decades in an unprecedented way (Zemp (2015)) but is also thought to play a dominant role over the 21st century (Meier *et al.* (2007)). The impacts of glacier loss are however not limited to sea-level rise but also include increasing geohazards (Richardson & Reynolds (2000)) and decreasing water availability (Kaser *et al.* (2010)). By now an anthropogenic signal in glacier mass balance can be detected with high confidence (Marzeion *et al.* (2014)). So it is worth having a look at the potential of semi-empirical models in capturing this contribution.

A promising dataset for testing this was published by Radić & Hock (2011) (RH). They projected 21st century mass balances for more than 120,000 glaciers and ice caps, upscaled to 19 regions containing all of the world's GICs (excluding the big ice sheets). They ran their model ten times with temperature and precipitation projections from ten global climate models. Unfortunately, many difficulties arise when looking at the model output in detail. First of all, it seems very strange that for most of the 10 model runs the projected rates of sea-level change from GIC melting decrease in the first few years and only then start to rise. This is counterfactual because, as mentioned above, today GICs loose mass in an accelerated, not decelerated, way and it seems highly unlikely that for the next degree of global warming this behaviour gets reversed. This is also not reproduced in later studies (Marzeion *et al.* (2012)). In figure 3.1 the rate of sea-level rise is plotted against temperature (not time), which makes the RT model a straight line. The effect of initially decreasing trends of sea-level rise can still be seen looking at the solid lines between zero and one degree C. If these first years are discarded in the semi-empirical calibration, the fit gets considerably better with the probability of a fit by chance decreasing by about one order of magnitude. One possibility to explain this unusual behaviour in the RH simulations is an initialization problem in their model but this could not be proved here. Besides this decrease in the rate in the first few years, six out of

the ten model runs show a more or less strong decrease later on (figure 3.1 solid line). This decrease might be explained by the gradual disappearance of GICs. Except for one of these six model runs (UKMO-HadCM3), which recovers later on, this seems plausible. But if this is the case, it remains unclear why such a behaviour can not be seen in the other model runs where temperatures also rise by more than 4°C relative to 2001. One model run (PCM) even shows a constantly decreasing rate of mass loss although temperature rises by 3.5°C over the 21st century. Here it might be suspected that the above postulated initialization problem does not level off or that precipitation gets overestimated.

Despite the partly rare behaviour of the RH projections, it is possible for each of the ten model runs to find semi-empirical parameters that give a good fit. A big problem, when it comes to interpreting the semi-empirical results, is that the mean equilibrium temperature T_0 of all ten model runs is around 4.3°C below the mean temperature of 2001. If the first 12 years are discarded for calibration, because of the above discussed potential initialisation issue, the equilibrium temperature is still 3°C below the 2001 reference value. But if this was true the GICs would not even have been stable in a pre-industrial climate. Figure 3.1 shows the rates of sea-level rise caused by GIC melting against temperature rise, for all 10 RH model runs, in solid lines. The semi-empirical fits are shown in dotted (VR) and dashed (RT) lines. For parameter calibration the first degree of warming compared to 2001 was discarded because of suspected initialization issues. To hindcast GIC mass changes for pre-industrial times the temperature was extended down to -1°C relative to 2001. Since in the VR model also $\mathrm{d}T/\mathrm{d}t$ is considered, in the fast response term, the GISS temperature (Hansen *et al.* (2010b)) is used for the hindcast. This results in a discontinuity at 0°C for some models which is not an issue for the RT model since it takes into account only T. Despite that the overall picture is the same: In most of the models glaciers would have lost mass even in a pre-industrial climate with rates as high as $\approx$ 1.3 mm/yr, which is unlikely and indeed counterfactual.

With the given GIC dataset it was hence not possible to get a physically consistent picture when applying two semi-empirical sea-level models. There are two possibilities to explain this. First of all, the sea-level models might

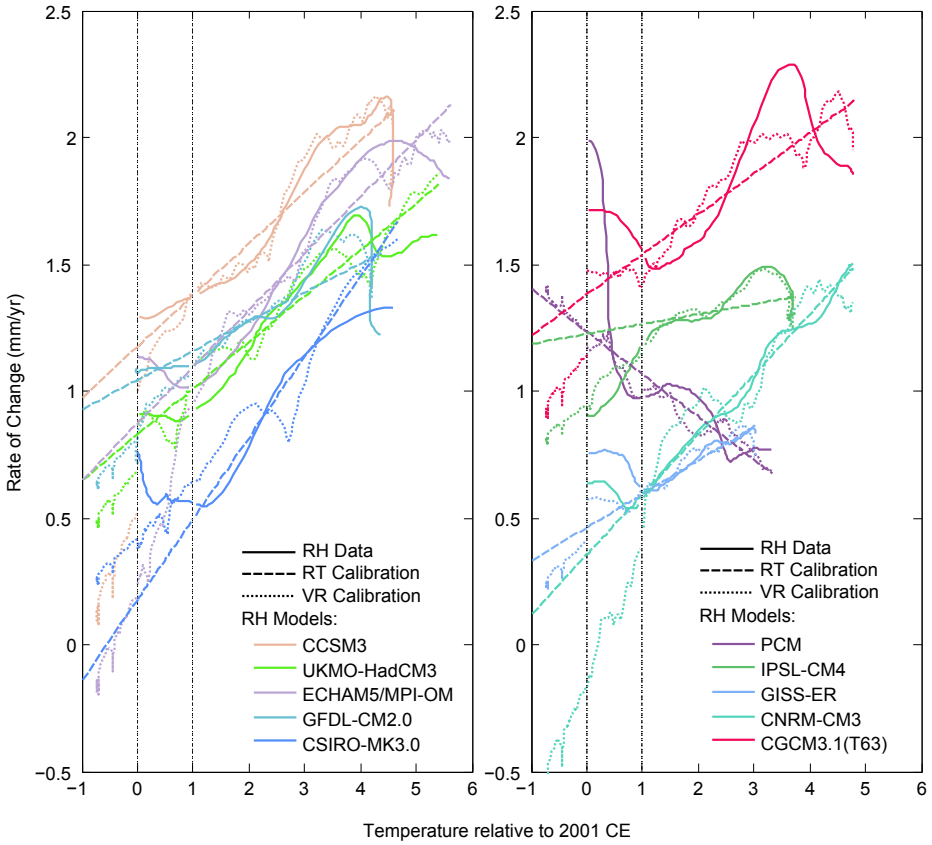

Figure 3.1: **Rate of sea-level change from GIC melting over temperature from Radić & Hock (2011) (RH) compared to semi-empirical model fits.** The different model runs of RH are indicated by different colours and labelled similar to the paper. Solid lines show the simulations of RH. Dotted lines show calibrations with the VR and dashed lines with the RT model. Because of the suspected problems with the RH data, discussed in the text, the first degree of warming is discarded for semi-empirical parameter evaluation. To hindcast pre-industrial times the temperature got extended to -1°C relative to 2001.

be too simplistic because they take into account only global, not local, temperature and no precipitation. The RH model, which also includes many semi-empirical parts, does take into account both and then upscales it to 19 regions. On the other hand, it might be suspected that many local differences level out if a global perspective is taken. Moreover temperature as sole input has the advantage that climate models do simulate it very well as opposed to precipitation (IPCC (2013)). The second possibility for the 'failure' of the tested semi-empirical models might of course be a weakness in the data basis. It is well known that the modelling of thousands of mountain glaciers to estimate their sea-level equivalent involves enormous difficulties and uncertainties. This can easily be illustrated when comparing the two estimates of global glacier ice by Raper & Braithwaite (2005) and Radić & Hock (2011) which differ by 0.36 m sea-level equivalent, giving 0.24 ± 0.03 m and 0.60 ± 0.07 m respectively. In this special case, it seems obvious that the ten models used by RH show some inconsistency in terms of peaking or even the sign of the trend in the rate of melting, independent of the total amount of GIC mass. The semi-empirical approach followed here could be another indicator that the simulations by RH might be flawed. Above, two possible sources of error were suggested, an initialization problem and an overestimation of precipitation by at least one model. Unfortunately, it was here not possible to recalculate the RH data, although a collaboration was initialized to do so.

Chapter 4

Testing the connection of sea level to temperature before 1100 CE

The observed correlation between sea level and temperature did not seem to hold prior to the year 1100 CE as pointed out by Kemp *et al.* (2011) and Rahmstorf *et al.* (2011). The reason is a clear step of 0.19°C in the EIV (error-in-variables) temperature of Mann *et al.* (2008) (MN08), comparing the periods 500–1000 CE and 1100–1400 CE, while the sea level of Kemp *et al.* (2011) (KE11) stays almost constant (see figure 4.1). Previous publications exploiting the semi-empirical link between temperature and sea level (Kemp *et al.* (2011), Rahmstorf *et al.* (2011), Schaeffer *et al.* (2012), Bittermann *et al.* (2013)) thus used to omit this early data. Two possible explanations for the discrepancy are: (i) errors in the temperature or sea-level data and (ii) an incorrect or imperfect model. As pointed out several times before (Kemp *et al.* (2011), Rahmstorf *et al.* (2011)) no linear, stationary and causal model connecting sea level and temperature could hindcast the discrepancy around 1100 CE. For an error in sea-level data to explain the misfit it would need to be outside the two sigma error margins (Kemp *et al.* (2011)) and is thus very unlikely. On the other hand, a temperature step of only around 0.2°C is well within the uncertainty of the MN08 temperature proxy series and therefore the most likely source for the misfit (although a combination of errors is also possible). Moreover, another statistical method (composite plus scale, CPS instead of EIV), also applied by Mann *et al.* (2008), yields a land-temperature reconstruction which is on average 0.2°C cooler before

1100 CE, but is in good agreement after 1100 CE (i.e. on average only 0.01°C cooler between 1100–1850 CE) - see figure 4.3. This can be interpreted as an additional source of uncertainty going along with the statistical method applied. Since only the EIV method yielded land-ocean temperatures, it is more appropriate for semi-empirical models, but a physical process simultaneously warming the ocean while keeping land temperatures constant before 1100 CE seems unlikely.

In this chapter another, at the time of the study, new temperature proxy series (Marcott *et al.* (2013)) is used to semi-empirically explain sea level for more than 2 millennia. Moreover, a better error representation of the temperature is introduced which relaxes the discrepancy of KE11 sea level and MN08 temperature before 1100 CE. By inverse modelling it is finally attempted to semi-empirically infer temperature from sea level, also strengthening the hypothesis that the step in the MN08 temperature around 1100 CE is in fact no physical signature. The observed connection of sea level and temperature apparently also holds prior to 1100 CE.

4.1 Refining the error representation

Previously (Kemp *et al.* (2011), Rahmstorf *et al.* (2011), Schaeffer *et al.* (2012), Bittermann *et al.* (2013)), the uncertainty in the temperature record was represented in every Monte Carlo (MC) sample draw by independently adding random values, sampled within the temperature uncertainty, for periods of ten years (see subsection 2.6 and Kemp *et al.* (2011)). To also take into account autocorrelation in the uncertainty, the yearly temperature is now, for each MC sample, treated as an auto-regressive process of order one (AR(1)) with the temperature proxy as its expectation value. Let $\tilde{T}_t$ be the AR(1)- and T_t the proxy temperature at time t with the AR(1) parameter α and white noise $\epsilon = N(0, \sigma_\epsilon^2)$. Then:

$$\tilde{T}_t \;=\; T_t + \alpha\,(\tilde{T}_{t-1} - T_{t-1}) + \epsilon. \tag{4.1}$$

The variance of $\tilde{T}$ which is $\sigma_\epsilon^2/(1-\alpha^2)$ as well as the other priors are taken to be the same as in Kemp *et al.* (2011). The AR(1) parameter is chosen to

resemble strong correlation ($\alpha = 0.99$), similar to chapter 5.

This way the autocorrelation in the randomly drawn $\tilde{T}_t$ more closely resembles autocorrelation in instrumental temperature data. As in Kemp *et al.* (2011), figure 4c, temperature and sea level get optimized at the same time. But while the optimized temperature given therein resembles pretty much the original proxy data because uncertainty was added as uncorrelated white noise, in this case it has the chance to deviate.

In panel (a) of figure 4.1, the selected AR(1) temperature is shown in red with grey uncertainty (5–95 % CI) and compared to the original Mann *et al.* (2008) EIV temperature in orange - both smoothed for visual clarity with a ssa filter of 15-year half-width. Clearly, the selected temperature is lower between 700–1100 CE, but also during the little ice age period (1500–1800 CE). The slightly higher temperature at the beginning of the record, which yields a rising sea level at that time, might imply that an AR(1) error is still an incomplete representation (Foster & Rahmstorf (2011)). Nevertheless, the average difference of 0.13°C between 700–1100 CE (maximal 0.24°C) suffices to explain 1,500 years of sea-level evolution also with the EIV temperature from Mann *et al.* (2008) as shown in figure 4.1 panel (b).

4.2 Calibration with Marcott et al. temperature

At the time of this study, Marcott *et al.* (2013) published proxy temperature reconstructions over the last 11,300 years, using different statistical methods. These reconstructions are not significantly different from the MN08 reconstruction, i.e. they agree well within their uncertainties (see figure 1 in Marcott *et al.* (2013)), but do not show a temperature step around 1100 CE as pronounced as in MN08. In the following, the RegEM (regularized expectation maximization) reconstruction is used. This is the most suited for our purpose, because it statistically fills data gaps, which becomes most important for the last centuries during which the proxy data network gets thinner and which is an important part of the calibration period. This reconstruction is on average 0.14°C cooler than the MN08 reconstruction between 500–1100 CE, while they are in good agreement afterwards (see also figure 4.3). As seen earlier, a temperature only 0.13°C lower than MN08 between

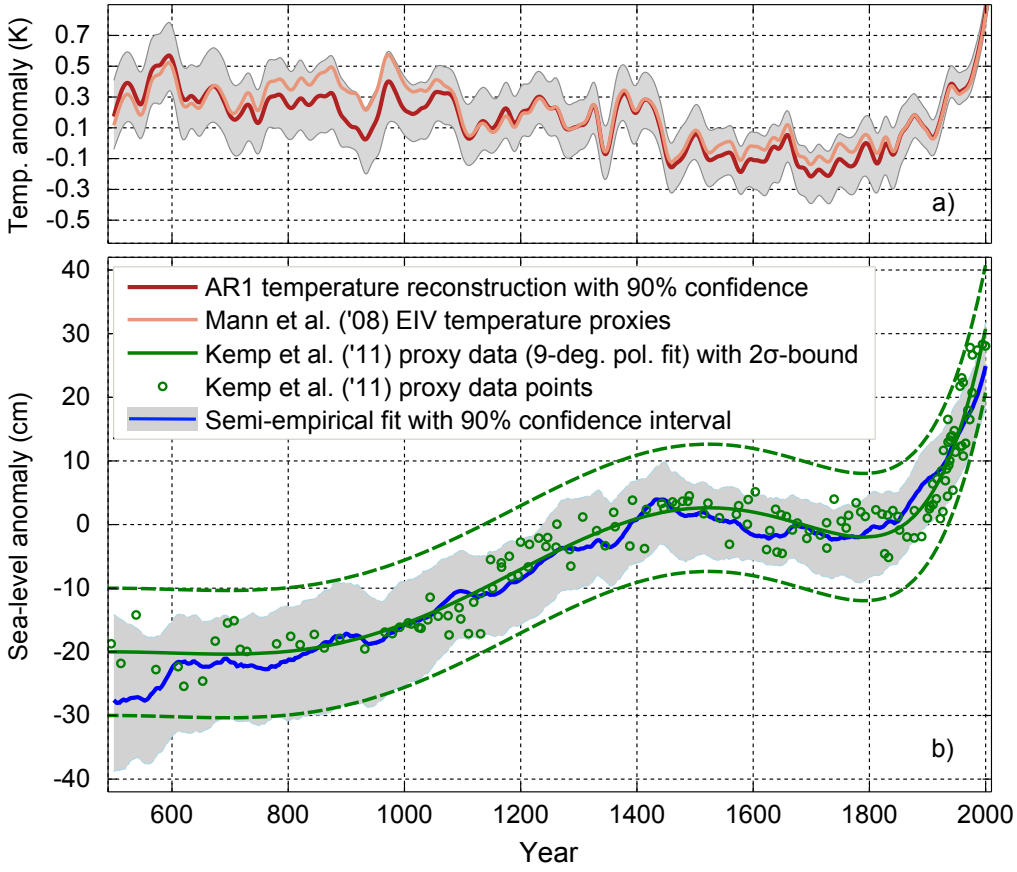

Figure 4.1: **Semi-empirical fit with AR(1) uncertainty representation for temperature data.** (a) The selected AR(1) temperature in red with grey uncertainty bar (5–95 % CI), compared to Mann *et al.* (2008) EIV temperature in orange - both time series filtered with 15-year half-width. (b) The resulting sea-level fit in blue with grey uncertainty compared to the Kemp *et al.* (2011) data points and a 9-degree polynomial.

700–1100 CE had been selected by the AR(1) model. Since the Marcott *et al.* (2013) RegEM data does not cover the whole instrumental period, we use the HadCRUT3v (Hadley Centre and the Climatic Research Unit Temperature 3v) instrumental data (www.cru.uea.ac.uk/cru/data/temperature/, Brohan *et al.* (2006)) from 1850 CE onward which is aligned with the proxy data over the period of overlap. To display common statistical properties, the instrumental data has been transformed to 20 year averages similar to the proxy data. The prior distribution used for the semi-empirical model is the same as the original one from Kemp *et al.* (2011) except that the noise added to the proxy temperature now resembles the uncertainty of Marcott RegEM. Figure 4.2 (panel (b) plot (i)) shows the semi-empirical sea-level reconstruction which is in very good agreement with the proxy data ($r^2 = 0.91$) if calibrated from 400 CE onwards. A rise in temperature of only approximately 0.04°C between 250–400 CE is not in accordance with the constant sea level before 400 CE. Therefore, as shown in figure 4.2 (panel (b) plot (ii)), the model performs slightly worse ($r^2 = 0.88$) if calibrated over the whole time period (-120–2000 CE), but still captures measured sea level within its uncertainty. Again, the above AR(1) error representation can be used for the temperature which will automatically select on average 0.1°C lower temperatures between 300–1100 CE and 1450–1800 CE. The resulting sea-level reconstruction, shown in figure 4.2 (panel (b) plot (iii)), resembles the proxy data very well ($r^2 = 0.90$).

Despite a small discrepancy of the Marcott *et al.* (2013) RegEM temperature and the sea-level data of Kemp *et al.* (2011) before 400 CE, the chosen semi-empirical model is able to explain over two millennia of sea-level changes and thus supports the observed relation of sea level and temperature also before 1100 CE.

4.3 Inverse modelling

The two examples above showed that a semi-empirical connection between sea level and temperature indeed holds true for 1.5 millennia if the MN08 temperature is modified slightly to reduce a temperature step around 1100 CE. The connection hold even longer (2100 years) if the Marcott *et al.* (2013)

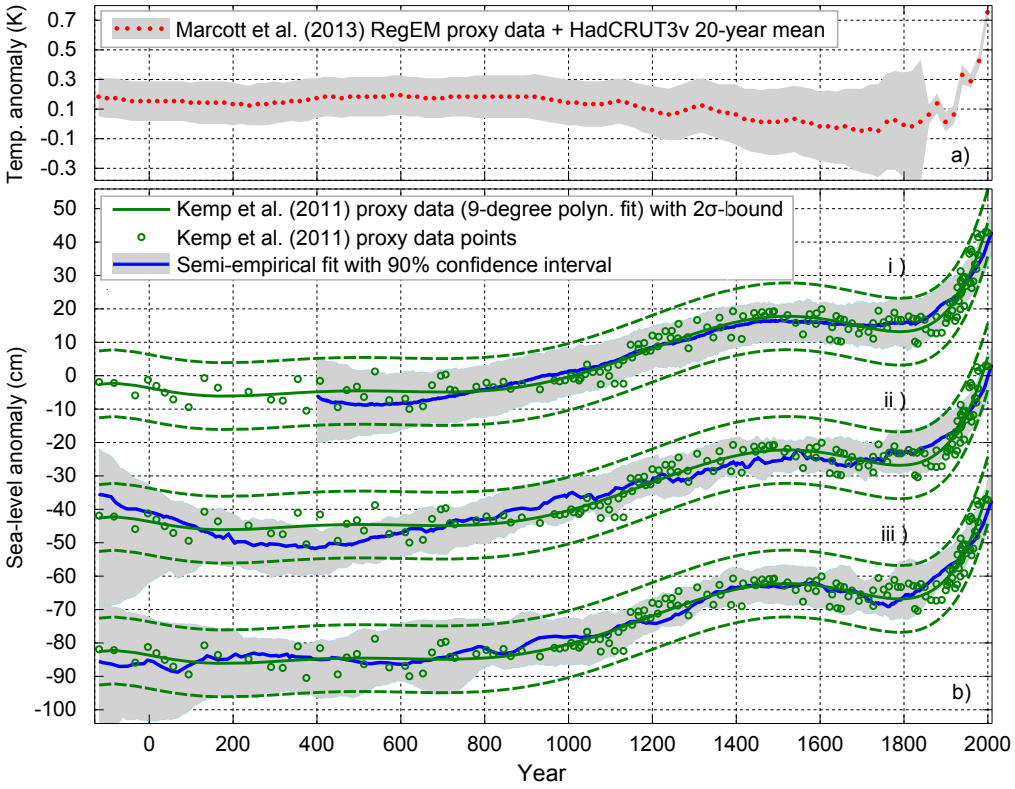

Figure 4.2: **Semi-empirical sea-level fit calibrated with the temperature of Marcott *et al.* (2013) and the sea level of Kemp *et al.* (2011).** (a) The temperature combination of Marcott *et al.* (2013) RegEM and HadCRUT3v (Brohan *et al.* (2006)) which was used as driver for the model. (b) Three model runs (arbitrary offset) with different calibration periods and temperature error representation. (i) Calibrated from 400 CE onwards with uncorrelated temperature error. (ii) Calibrated from -120 CE onwards with uncorrelated temperature error. (iii) Calibrated from -120 CE onwards with AR(1) temperature error.

temperature data is used. It is now also possible to directly infer temperature from sea level by solving equation 1.3 for temperature. This is done numerically for time steps i and yields the discretized equations 4.2 and 4.3:

$$T_i = \frac{\Delta h_i + a_1\, T^{00} + a_2\, T^0_{i-1}\,(1 - \Delta t_i/\tau)}{a - a_2\,(\Delta t_i/\tau)} \tag{4.2}$$

$$T^0_i = \frac{T_i - T^0_{i-1}}{\tau}\,\Delta t_i + T^0_{i-1} \tag{4.3}$$

$$\Delta x_i = x_i - x_{i-1}$$

Because the used sea level is unevenly sampled, noisy proxy data, and $T \propto \Delta h$, the resulting temperature is bound to be even more noisy. Therefore, to smooth the sea-level data, polynomials were chosen. To represent the sea-level variance, for each MC sample each data point is first randomly sampled within its time and sea-level uncertainties before calculating a 7-degree polynomial from all sea-level data points. As calibration target the MN08 temperature is used from 1100 CE onwards and thus, the temperature before 1100 CE gets hindcasted. For the simulation shown in figure 4.3a similar, uninformative, prior distributions as in Bittermann *et al.* (2013) (chapter 2) were used. The simulation proved to be sensitive to the prior chosen for T^0_1 as well as the calibration period. Therefore, T^0_1 was conservatively chosen to be $T^0_1 \equiv \mathcal{N}(0, (0.3°\mathrm{C})^2)$ relative to the first hundred years of the calibration period. Although different priors alter the hindcast, the results are robust within their uncertainties and all show the same pattern (figure 4.3) which is a constant or slowly falling temperature until around 800 CE, a slight increase or plateau until around 1200 CE, and a temperature decrease until around 1700 CE followed by a sharp increase. These different periods coincide well with a constant or slightly decreasing preindustrial temperature (Marcott *et al.* (2013)), interrupted by the medieval climate anomaly (MCA, 950–1250 CE) and the little ice age (LIA, 1400–1700 CE) (Mann *et al.* (2009)) at the end of which man-made climate warming sets in. The length of the calibration period is important, especially the inclusion of the temperature decrease in the MN08 data between 1400–1500 CE. Without including this period, the hindcasts show a much flatter temperature evolution before 800 CE, while the signatures of MCA and LIA are still

present. Although these hindcasts are sensitive to certain conditions, they all show the same pattern and coincide within their uncertainties. Foremost, they exclude, with >90% confidence, a sudden drop in temperature around the year 1100 CE (Mann *et al.* (2008) EIV) and a temperature rise between 250–400 CE (Marcott *et al.* (2013) RegEM), also within their uncertainty.

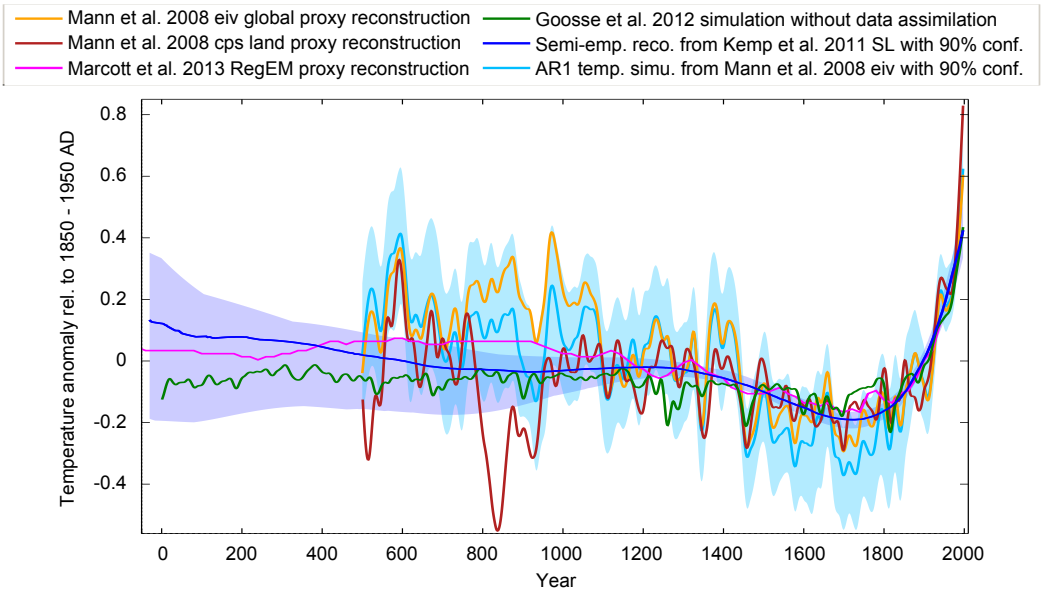

Figure 4.3: **Temperature simulations and reconstructions.** Comparison of the above semi-empirical temperature simulations (light and dark blue) to different temperature proxies (Mann *et al.* (2008), Marcott *et al.* (2013)) and a simulation (Goosse *et al.* (2012)).

4.4 Conclusions

Summarizing, it could be shown that previous problems calibrating the semi-empirical sea-level model from Kemp *et al.* (2011) with the sea-level data therein and the Mann *et al.* (2008) EIV proxy data from before 1100 CE dissolve if a simple AR(1) error model with high correlation is applied to the temperature proxy data. The model then automatically selects temperatures which are on average lower than the Mann et al. EIV temperature before 1100 CE and thus yields correct reconstructions. Using Marcott *et al.* (2013) RegEM global temperature data, faithful reconstructions of sea-level history from 400 CE onwards ($r^2 = 0.91$) and -120 CE onwards ($r^2 = 0.88$) are pos-

sible. By additionally applying an AR(1) error model on the Marcott *et al.* (2013) temperature, over two millennia of sea-level history can be reconstructed with even higher fidelity ($r^2 = 0.90$). Finally, by inverse modelling, i.e. semi-empirically inferring temperature from sea level, the proposition that the drop of approximately 0.2°C in the Mann *et al.* (2008) EIV temperature around 1100 CE is not a true physical signature could be substantiated with >90% confidence. Inferring from this model and the Kemp *et al.* (2011) sea-level data, it is likely that the temperature before 1100 CE is more probably closer to the lower edge of the uncertainty interval of Mann *et al.* (2008). Overall it shows that indeed the observed connection of sea level and temperature holds also before 1100 CE.

Chapter 5

Common Era sea level

Up to date global sea level records (figure 1.2) did not span more than 300 years (Jevrejeva *et al.* (2008)) with most of them starting only between 1850-1900 CE (Church & White (2006), Church & White (2011), Ray & Douglas (2011), Wenzel & Schröter (2014), Hay *et al.* (2015)). For long term, high resolution reconstructions either model hindcasts (Grinsted *et al.* (2009)) or local sea-level reconstructions (Kemp *et al.* (2011)) have been used (figure 5.1a). The deviation of local, North Carolina sea-level from global sea level was estimated to be $\pm$ 10 cm (Kemp *et al.* (2011)). As more recent salt marsh reconstructions from the US east coast show this might have been an underestimation. As shown in figure 5.2 panel (b) there are strong differences even in close by local sea-level records. Especially the comparison of the North Carolina and New Jersey record indicate strong dynamic sea-level effects, possibly due to changes in the Gulf Stream (Yin & Goddard (2013)) or near-shore wind stress (Woodworth *et al.* (2014)). Changes in the Gulf Stream might include a shift of the Gulf Stream, a change in ocean density contrast across the Gulf Stream (Yin & Goddard (2013)) or a change in the Gulf Stream strength. In the geostrophic approximation, a weakened Gulf Stream would raise sea level north of Cape Hatteras (New Jersey) relative to the south (North Carolina). The Gulf Stream is also a major source of heat transport from the south to the north (Feulner *et al.* (2013)) so a weakened stream would leave its traces in the hemispheric temperature difference. A hint that something like this might have happened gives the continental-scale temperature reconstruction of Ahmed (2013), the hemispherical tempera-

ture difference of which is plotted in figure 5.2 panel (a). A clear deviation from zero can be seen approximately simultaneously to the divergence of New Jersey and North Carolina sea level, plotted in figure 5.2 panel (b). As mentioned above more than one mechanism can possibly explain the sea-level difference. So this purely qualitative comparison of hemispheric temperature differences might be seen as a hint only, which is not in line with the long term Atlantic meridional overturning circulation proxy by Rahmstorf *et al.* (2015), who find a different pattern, especially in the last approximately 100 years. A more detailed study is necessary to entangle the possible processes here.

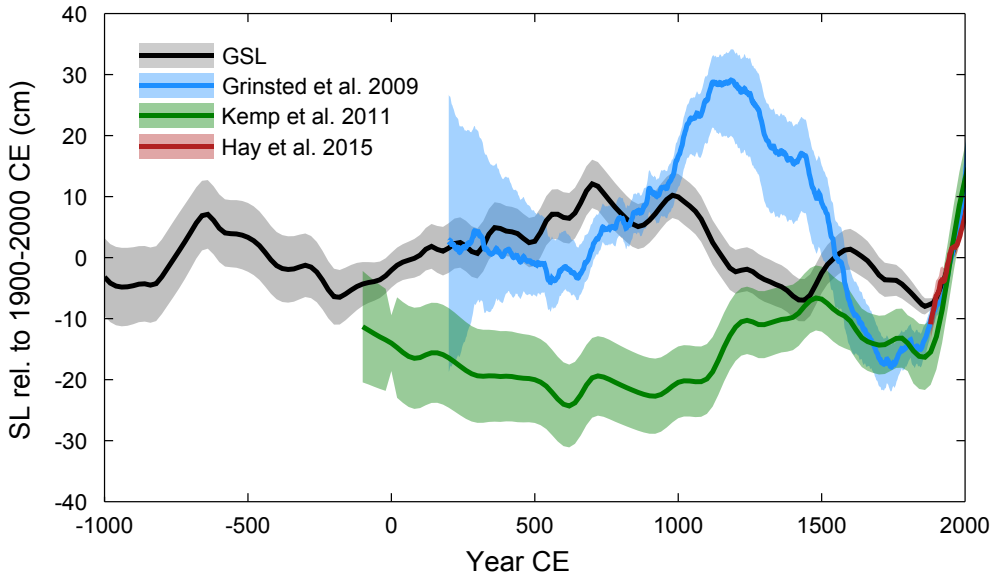

Figure 5.1: **Comparison of sea-level reconstructions.** Comparison of sea-level reconstructions used as approximation of global sea level in literature. GSL denotes the reconstruction presented here and in Kopp *et al.* (2016). The other reconstructions are from references Grinsted *et al.* (2009), Kemp *et al.* (2011), Hay *et al.* (2015). The model hindcast (Grinsted *et al.* (2009)) shows the Moberg reconstruction from their figure 7b. Uncertainties represent one standard deviation and the reference period is 1850–2000 CE.

A statistical synthesis of local proxy records, which already is a common practice for temperature records (Mann *et al.* (2008)), has never before been undertaken for sea-level records. To analyse Common Era sea-level variability Kopp *et al.* (2016) performed an empirical Bayesian meta-analysis of 21

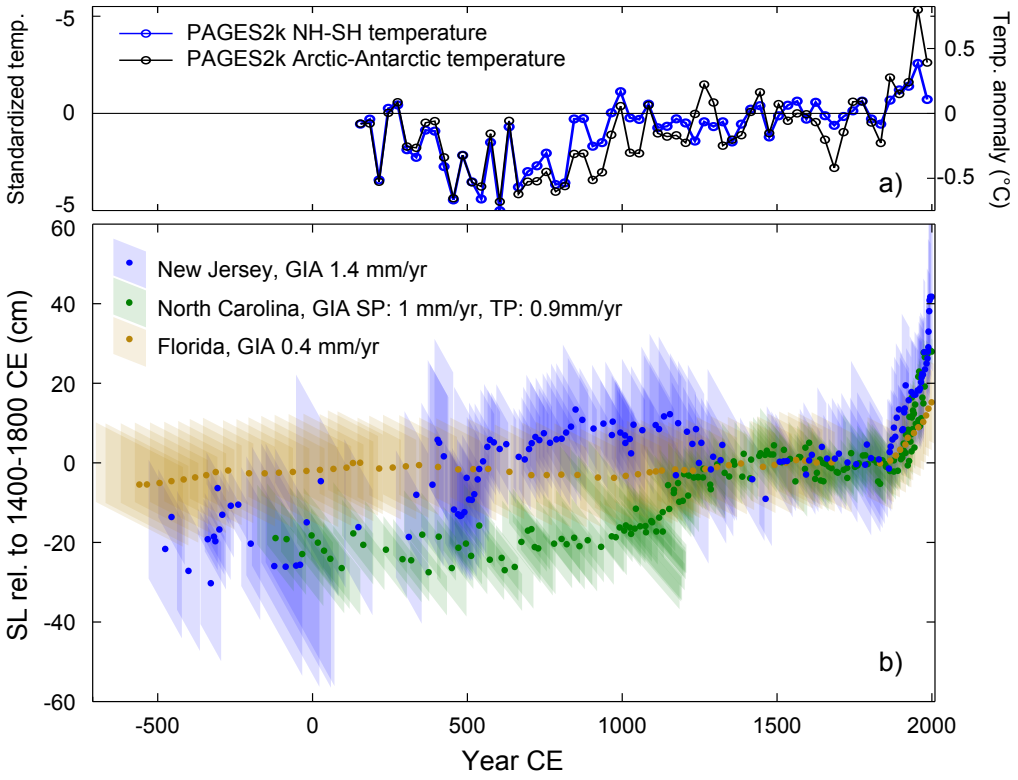

Figure 5.2: **US east-coast sea-level proxies and hemispheric temperature difference.** (a) Hemispheric temperature difference as well as Arctic-Antarctic temperature difference from the Ahmed (2013) data. The two y-axis scales give the standardized temperature used in Ahmed (2013) as well as a conversion by eyesight to °C as done in their figure 4b. (b) Comparison of local sea-level reconstructions from the United States east coast, corrected for the given rate of glacial isostatic adjustment (Kemp *et al.* (2011), Kemp *et al.* (2013), Kemp *et al.* (2014)). The reference period is 1400–1800 CE.

relative sea-level (RSL) reconstructions together with an additional 66 tide-gauge records spanning approximately the last 3000 years and 300 years respectively. Similar to temperature compilations, distinct periods of climate variability can be found in the compiled global sea-level (GSL) record (figures 5.1 and 5.3a). Most notably there is a decline of 0.4 ± 0.2 mm/yr over the period 1000–1400 CE which coincides with the transition into the little ice age (LIA). In th industrial era GSL rose in every 40-year period since 1860 CE. Moreover the rate of 20th century sea-level rise exceeds any rate since at least -700 CE with a probability $P \geq 0.95$.

To globally synthesise proxy and tide-gauge records to one sea-level field $f(\mathbf{x}, t)$ it was modelled as a superposition of three components which depend on spatial location $\mathbf{x}$ and time t:

$$f(\mathbf{x}, t) = g(t) + l(\mathbf{x})(t - t_0) + m(\mathbf{x}, t) \tag{5.1}$$

These three components are: (1) A globally uniform field $g(t)$ representing thermal expansion and land-ice lost. (2) A local, regionally varying component of constant rate $l(\mathbf{x})(t - t_0)$ which can represent slowly changing factors such as glacial isostatic adjustment (Peltier (2004)), tectonics and natural sediment compaction. (3) A locally and temporally varying field $m(\mathbf{x}, t)$, representing ocean/atmosphere dynamics (Yin & Goddard (2013)) as well as the gravitational, elastic, and rotational 'fingerprint' effects of water mass redistribution (Mitrovica *et al.* (2011), Kopp *et al.* (2015)). Each of the components has priors that are again characterized by hyper-parameters giving the amplitude as well as temporal and spatial scales of variability. The shape of five different hyper-parameters can be seen in the Supplementary Information of Kopp *et al.* (2016). Sea-level records used for this synthesis are globally not equally distributed but the spatially correlated terms $l(\mathbf{x})(t - t_0)$ and $m(\mathbf{x}, t)$ ensure that certain regions with high density of records do not get weighted more than others. There however remains a ambiguity of a linear trend ($\approx \pm 0.1$ mm/yr) that might be present at all reconstruction sites used without being a truly global trend. This means, that it can not fully be ruled out that by coincidence all sites show a trend in RSL that the model accounts for as a GSL trend. However this will not be a problem for the

semi-empirical model, as discussed later, but needs to be coped with for the GSL reconstruction. So for the GSL compilation $g(t)$, used in the following, and shown in figures 5.1 and 5.3a, this ambiguity was resolved by putting the mean GSL during the periods -100–100 and 1600–1800 CE on the same level (Kopp *et al.* (2016)). This is important to keep in mind when interpreting the GSL compilation, the focus of which is on sub-millennial variations since a long term trend was not allowed. It can thus not be argued that GSL was higher between 700–1000 CE than today, judging from figures 5.1 and 5.3a, because a trend of only 0.1 mm/yr could make a difference of 0.1 meter over 1000 years. Robust key features of this GSL are a rise between 0–700 CE (0.2 ± 0.1 mm/yr), a drop between 1000–1400 CE (0.4 ± 0.2 mm/yr), and another rise starting in the 19th century (0.4 ± 0.6 mm/yr from 1860–1900 CE, 1.4 ± 0.2 mm/yr over the 20th century). The rise and drop in GSL between 1400–1600 and 1600–1800 CE are significant but depend on data from the north-west Atlantic.

As already mentioned above the reconstructed GSL shares common features with global temperature reconstructions on multi-century timescales. The drop in GSL between 1000–1400 CE for example coincides with a ≈ 0.2°C decrease in global temperature (Mann *et al.* (2009), Marcott *et al.* (2013)). This accordance is the prerequisite for the use of semi-empirical sea-level models. The semi-empirical sea-level model used for this study relates the rate of GSL change $\mathrm{d}h/\mathrm{d}t$ to global mean temperature $T(t)$:

$$\begin{aligned} \mathrm{d}h/\mathrm{d}t &= a\Big(T(t) - T_0(t)\Big) + c(t) \\ &\text{with} \\ \mathrm{d}T_0(t)/\mathrm{d}t &= (T(t) - T_0(t))/\tau \\ \mathrm{d}c(t)/\mathrm{d}t &= -c/\tau_c. \end{aligned} \tag{5.2}$$

where a is the sensitivity of the GSL rate to a deviation of $T(t)$ from an equilibrium temperature $T_0(t)$, τ is the timescale on which the equilibrium temperature decays toward the actual temperature, and c is a temperature-independent rate term decaying on the timescale τ_c. The major difference to equation 1.3, used in Bittermann *et al.* (2013), is the substitution of the a_1 term with $c(t)$ which eliminates the temperature dependence in this term.

This constant rate term has the advantage that it resolves the above mentioned ambiguity in the rate of sea-level rise. So an additional rate of $\approx \pm 0.1$ mm/yr will be confined to c while the other parameters stay unaffected. Sea-level projections thus have the same ambiguity as the GSL record but their responses to temperature remain unchanged. Similar to chapter 2 and Bittermann *et al.* (2013) also the fast response term used in the semi-empirical formulation of Kemp *et al.* (2011) was dropped because it can not be resolved. After having calibrated the model with GSL (figure 5.3a) and two different proxy temperatures (figure 5.3b) the semi-empirical fit shown in figure 5.3c is obtained. With the corresponding posterior parameter distribution (figure 5.4 and table 5.4) one can try to estimate the anthropogenically caused amount of GSL rise as well as future GSL rise under certain scenarios. For further information on the model and model calibration see the methods subsection 5.4 below.

5.1 Anthropogenic 20th century sea-level rise

In order to assess the anthropogenic part of the observed 20th-century GSL rise two alternative global temperature histories without global warming are applied to drive GSL. Scenario 1 assumes that the 500–1800 CE trend in the proxy temperatures is representative of Earth's late Holocene cooling (Marcott *et al.* (2013)) and that, without anthropogenic warming, temperature would have returned to this trend in 1900 CE. In scenario 2 temperature stabilizes at its 500–1800 CE mean after 1900 CE. The difference of sea level under observed (Brohan *et al.* (2006)) and the two counterfactual temperature scenarios can hence be understood as the anthropogenic part of 20th century GSL rise.

Figure 5.5 shows the 20th century sea-level hindcasts under both counterfactual temperature scenarios as well as the historical scenario. A summary is given in tables 5.1 and 5.2 as well as figure 5.3a. What becomes clear is that the human influence dominates 20th century sea-level rise which is in accordance also with other studies (Jevrejeva & Moore (2009), Becker *et al.* (2014), Dangendorf *et al.* (2015)).

Consistent with an observed 20th century GSL rise of 13.8 ± 1.5 cm the

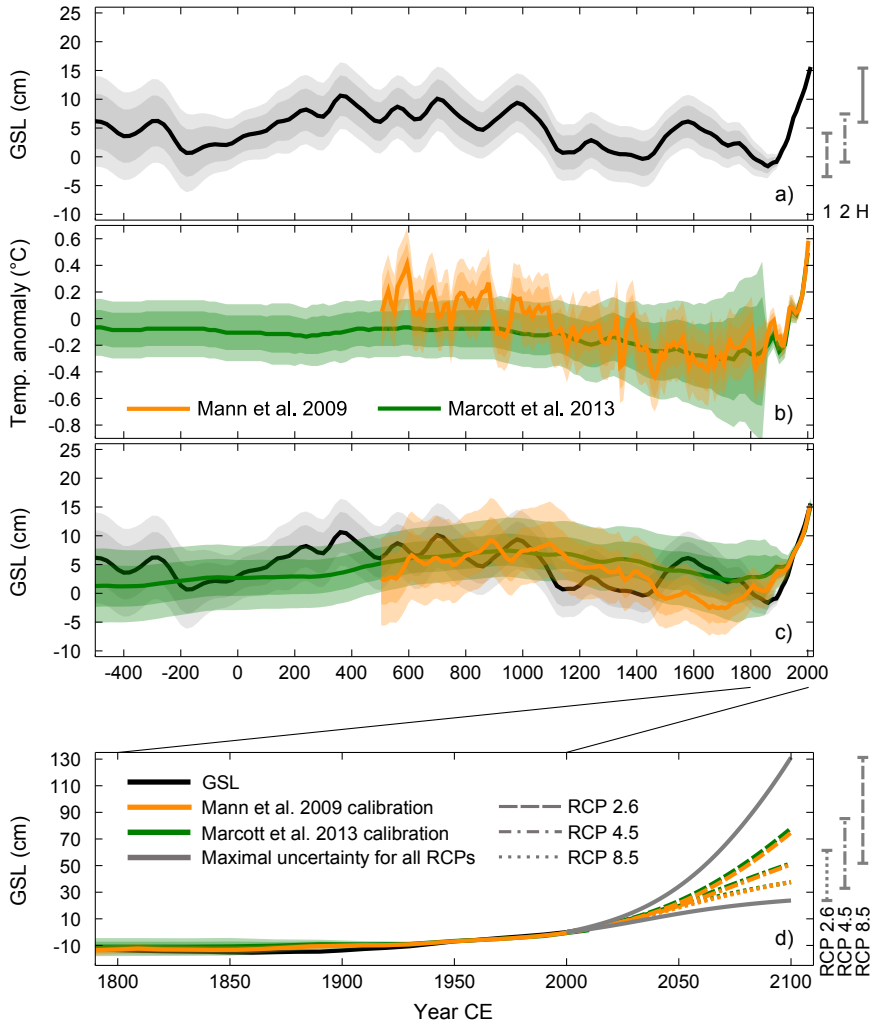

Figure 5.3: **Semi-empirical calibration and projections of GSL** (a) Global sea-level reconstruction relative to 1900 CE. Bars on the right show 20th century sea-level rise under a historic scenario (H) as well as two counterfactual scenarios without global warming (90% interval of both calibrations). (b) Temperature proxy reconstructions (Mann *et al.* (2009), Marcott *et al.* (2013)) used for calibration. Temperatures are given relative to the mean of 1850–2000 CE (see methods section 5.4) (c) Semi-empirical fits to GSL using the two temperature reconstructions shown in the panel above. (d) Same as panel (c) with additional 21st century sea-level projections under RCPs 2.6, 4.5 and 8.5. The bars on the right give 90% confidence intervals for GSL in 2100 relative to 2000 CE. GSL in panel (a) and (c) are given relative to 1900 CE while panel (d) is plotted relative to 2000 CE. Heavy shadings in all panels symbolizes 67% confidence while light shadings show the 90% confidence intervals.

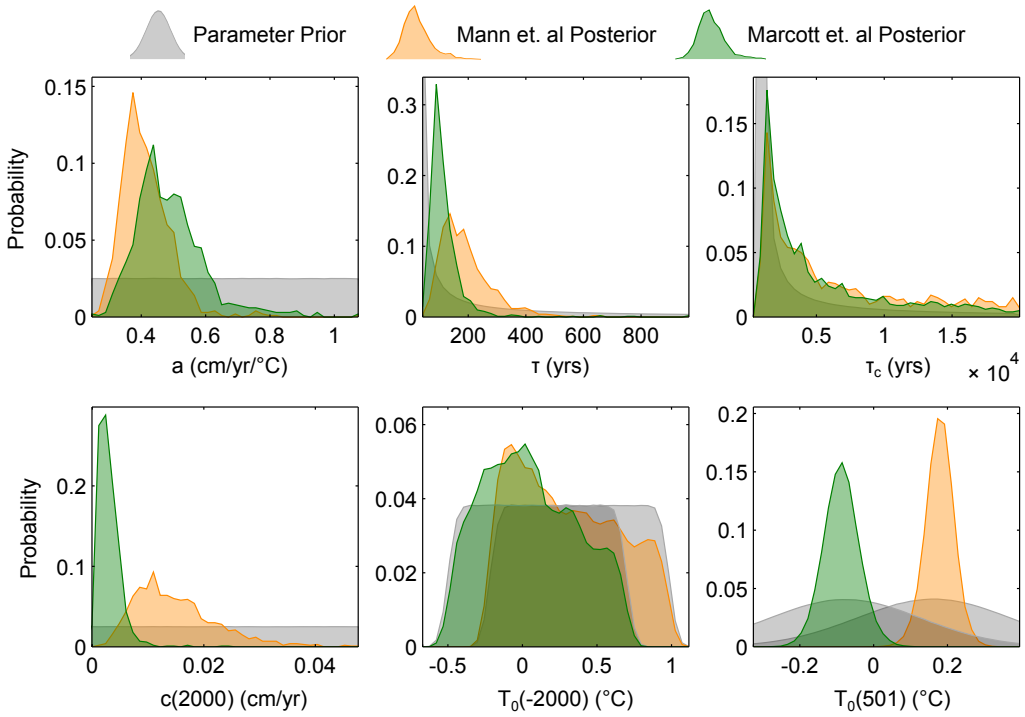

Figure 5.4: **Prior and posterior parameter distributions.** Probability distributions of the semi-empirical parameters from equation 5.2. Prior distribution are shown in grey but not fully if that would obscure posterior distributions (see also table 5.4). The green and orange distributions represent the posterior distributions after a calibration with Marcott *et al.* (2013) and Mann *et al.* (2009) temperatures respectively. See also table 5.4.

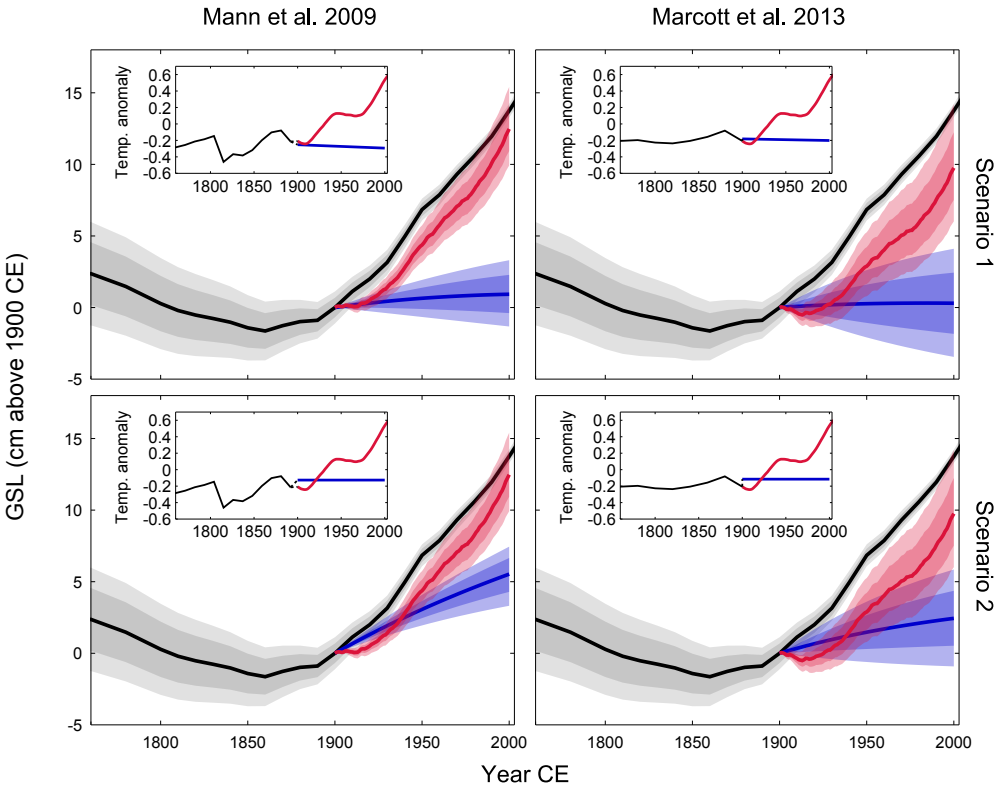

Figure 5.5: **GSL under observed and two counterfactual temperature scenarios without anthropogenic warming.** The left/right column shows model calibration with the Mann *et al.* (2009)/Marcott *et al.* (2013) temperature (see inset). The upper/lower row shows sea-level under counterfactual scenario 1/2, described in the text. In the insets, the black curve represents the temperature proxy reconstruction used for calibration while the red line represents the observed 20th century HadCRUT3 temperature Brohan *et al.* (2006). The blue line in the inset represents the two counterfactual temperature scenarios without anthropogenic warming. In the main plots the GSL from figure 5.3a is shown in black while red and blue give 20th century sea level under the temperature scenarios from the insets (see also table 5.1). The difference of red and blue might thus be understood as the anthropogenic part of GSL rise. Heavy shadings indicate a 67% and light shadings a 90% confidence.

Table 5.1: **Hindcasts of 20th century global sea-level rise (cm).** The 20th century hindcasts are calculated from observed temperature (Brohan *et al.* (2006)) as well as two counterfactual temperature scenarios described in the text and shown in figure 5.5. All values are given relative to 1900 CE. Summary results show minima of lower bounds, and maxima of upper bounds of both temperature calibrations.

	Summary		Calibrated to: Mann *et al.* (2009)		Marcott *et al.* (2013)	
Quantile	50	5–95	50	5–95	50	5–95
Observed	13.8	12.6–15.0				
Historical	11.1	6.0–15.4	12.5	9.9–15.4	9.8	6.0–14.2
Scenario 1	0.6	-3.5–4.1	0.9	-1.3–3.3	0.3	-3.5–4.1
Scenario 2	4.0	-0.9–7.5	5.5	3.3–7.5	2.4	-0.9–5.9
Percent of historical:						
Scenario 1	6	-32–51	8	-11–26	3	-32–51
Scenario 2	35	-13–59	44	28–59	25	-13–49

Table 5.2: **Significance level on which the observed GSL rise since 1900 CE exceeds the counterfactual projections.**

	Scenario 1 calibrated against:		Scenario 2 calibrated against:	
Year	Mann *et al.* (2009)	Marcott *et al.* (2013)	Mann *et al.* (2009)	Marcott *et al.* (2013)
1910	0.34	0.20	0.00	0.00
1920	0.70	0.33	0.01	0.01
1930	0.96	0.54	0.15	0.14
1940	1.00	0.75	0.68	0.64
1950	1.00	0.88	0.96	0.95
1960	1.00	0.93	0.99	0.99
1970	1.00	0.95	1.00	1.00
1980	1.00	0.97	1.00	1.00
1990	1.00	0.98	1.00	1.00
2000	1.00	1.00	1.00	1.00

semi-empirical hindcast, driven by historical temperatures, is 13 cm, with a 90% confidence interval of 7.7–17.5 cm. In absence of global warming it is very likely, with $P = 0.90$, that only -32–51 % (Scenario 1) or -13–59 % (Scenario 2) of 20th century GSL rise would have happened (see table 5.1). This means that, summarizing both scenarios, GSL would not have exceeded 59 % of the observed 20th century rise and could even have sunken by about one third. Summarizing both calibration and counterfactual temperature scenarios, observed sea level has likely ($P \geq 0.83$) surpassed sea level without global warming by 1950 CE and extremely likely ($P \geq 0.95$) by 1970 (see table 5.2).

These results confirm and give further strength to the notion that most of the observed GSL rise is caused by human induced climate change. The anthropogenic GSL contributions presented here are similar to Jevrejeva & Moore (2009) who estimated a non-anthropogenic GSL rise of 1–7 cm. They however calibrated their semi-empirical model to tide-gauge data only, the results might thus not be considered as robust as the ones presented here. Also Becker *et al.* (2014) came to a similar conclusion, namely that it is extremely likely that less than 30 % of sea-level rise between 1880–2002 CE could be explained by natural variability. They also used tide-gauge records only and could thus be biased low. A more recent study by Dangendorf *et al.* (2015) concluded it virtually certain with $P = 0.99$ that $\geq$ 45 % of the observed GSL rise is of anthropogenic origin. All those studies differ in their methods and the record lengths used. With a length of 3000 years, this study uses by far the longest record and can thus provide a high confidence in the numbers presented.

5.2 21st century sea-level rise projections

With the same calibrated semi-empirical model it is possible to calculate GSL under certain future emission scenarios the so called Representative Concentration Pathways (RCPs, Van Vuuren *et al.* (2011)). From the emissions given by these scenarios global mean temperature can be calculated to again drive the semi-empirical model. Three RCPs (RCP 2.6, RCP 4.5 and RCP 8.5) are considered here, named after the additional radiative forcing in W/m^2 by 2100 CE relative to pre-industrial. RCP 2.6, 4.5 and 8.5 correspond to very strong greenhouse gas mitigation, moderate greenhouse gas mitigation and a high-end business as usual scenario, respectively. The resulting ranges of GSL rise are given in table 5.3. The very likely ranges ($P = 0.90$) of GSL rise by 2100 CE, relative to 2000 CE, are: 24–61 cm, 33–85 cm and 51–131 cm for the RCPs 2.6, 4.5 and 8.5. Even though the ocean is a very inert part of the climate system, i.e. a slowly responding part, these numbers indicate that, with strong emissions abatement, a 26–70 cm rise of sea level could be prevented by 2100 CE. Yet these projections should be seen as a lower limit since they might underestimate GSL rise if new processes, not active during

Table 5.3: **Projections of 21st century global sea-level rise (cm).** Comparison of previous studies that were using different methods. All values are given relative to 2000 CE except AR5, which is relative to the 1985–2005 CE average.

Method	IPCC (2013) AR5 assessment		Schaeffer *et al.* (2012) semi-empirical		Kopp *et al.* (2014) bottom-up			Horton *et al.* (2014) survey	
Quantile	50	17–83	50	5–95	50	17–83	5–95	17–83	5–95
RCP 2.6	43	28–60	75	52–96	50	37–65	29–82	40–60	25–70
RCP 4.5	52	35–70	90	64–121	59	45–77	36–93	not asked	
RCP 8.5	73	53–97	not calculated		79	62–100	55 – 121	70–120	50–150

This study: showing both calibrations and a summary of results across both temperature calibrations giving the median of medians, minima of lower bounds, and maxima of upper bounds.

Calib. Temp.	Summary			Mann *et al.* (2009)			Marcott *et al.* (2013)		
Quantiles	50	17–83	5–95	50	17–83	5–95	50	17–83	5–95
RCP 2.6	38	28–51	24–61	38	29–50	25–59	38	28–51	24–61
RCP 4.5	51	39–69	33–85	51	39–66	34–81	52	39–69	33–85
RCP 8.5	76	59–105	51–131	75	59–99	52–121	78	60–105	52–131

the calibration period, start acting in the 21st century. Dynamic ice sheet processes for example have the potential to raise sea level considerably over the course of centuries to millennia (Joughin *et al.* (2014), Mengel & Levermann (2014), Robinson *et al.* (2012)) and would not have been captured by the semi-empirical model. Theses projections are lower compared to most other semi-empirical projections (Moore *et al.* (2013)) also from a similar model calibrated against North Carolina relative sea level (Schaeffer *et al.* (2012)). But they are in good agreement with the AR5 (IPCC (2013)) process-based projections, which themselves increased compared to AR4 (IPCC (2007)), as well as bottom-up probabilistic projections from Kopp *et al.* (2014) (table 5.3). This convergence of very different kinds of models strengthens the confidence in the individual projections.

5.3 Conclusions

Using a newly reconstructed global sea-level record over the Common Era (Kopp *et al.* (2016)) a semi-empirical model was successfully calibrated with two different temperature proxies (Mann *et al.* (2009), Marcott *et al.* (2013)) as shown in figure 5.3a-c. With this calibrated model the anthropogenic 20th

century global sea-level rise was estimated as the difference between sea-level rise under historic temperature pathway and two counterfactual temperature scenarios without anthropogenic global warming (figure 5.3a). It shows to be extremely likely ($P = 0.95$) that more than 40 % of the observed GSL rise can be credited to human-induced global warming. Projecting 21st century sea level under different climate change scenarios (RCPs) largely reconciles the difference between process-based and semi-empirical models. The very likely ($P = 0.90$) levels of GSL projected here are, 51–131 cm under RCP 8.5 (business as usual), 33–85 under RCP 4.5 (moderate greenhouse gas mitigation) and 24–61 cm under RCP 2.6 (very strong greenhouse gas mitigation) (see table 5.3 and figure 5.3d).

5.4 Methods

The semi-empirical model, which is defined by equation 5.2, is calibrated using a Metropolis-Hastings (MH) algorithm (Hastings (1970)). After determining a maximum likelihood parameter set $\mathbf{\Psi} = \{c(t), T_0(t), a, \tau_1, \tau_2\}$, the MH algorithm samples from the posterior distribution $P(\mathbf{\Psi}|g(t), T(t))$. The first 1000 samples are discarded in a so called burning-in period and the Markov chain is then thinned to every 500th sample to eliminate autocorrelation in the posterior samples. The final sample size is $m = 1000$.

As temperature input $T(t)$ two alternative proxy reconstructions $S(t)$ (figure 5.3b) with added noise ($\mathbf{S} \sim \mathcal{N}(\mathbf{T}, \Omega)$) are used. Plotted in orange in figure 5.3b is an 11-year average of the Mann *et al.* (2009) RegEM CFR (Regularized Expectation Maximization Climate Field Reconstruction) temperature which incorporates the HadCRUT3 instrumental global temperature (Brohan *et al.* (2006)). The green curve in figure 5.3b shows the second temperature used, namely the Marcott *et al.* (2013) RegEM global reconstruction. The Marcott temperature is reported as 20-year average values and was, for the purpose here, combined with 20 year-average values of the instrumental HadCRUT3 temperature (Brohan *et al.* (2006)), by aligning the two data sets over the period of overlap (1850–1940 CE). The reason for complementing the Marcott proxy reconstruction with instrumental data is that the number of individual proxy data used for the reconstruction

decreases towards present and thus the uncertainty increases. Both temperatures are generally in good agreement, with the Marcott *et al.* (2013) data showing ≈ 0.2°C lower temperatures before 1100 CE (see chapter 4.2). Because of these differences it makes sense to use both temperature time series for a more realistic uncertainty estimation while the general agreement provides confidence that the true global temperature is represented within the uncertainties of these records. To estimate the covariance matrix Ω of the proxy reconstructions $\mathbf{S}$, which is not given for either temperature proxy, $\mathbf{S}$ is assumed to be an AR(1) (auto regressive process of order 1) time series with a correlation e-folding time τ_{ar1} of ten years and a variance as given by the reconstruction. As shown in figure 5.6, $\tau_{ar1} = 10yrs$ was chosen because the resulting autocorrelation of $\mathbf{T}$ very well resembled the autocorrelation in the detrended instrumental data of Cowtan & Way (2014).

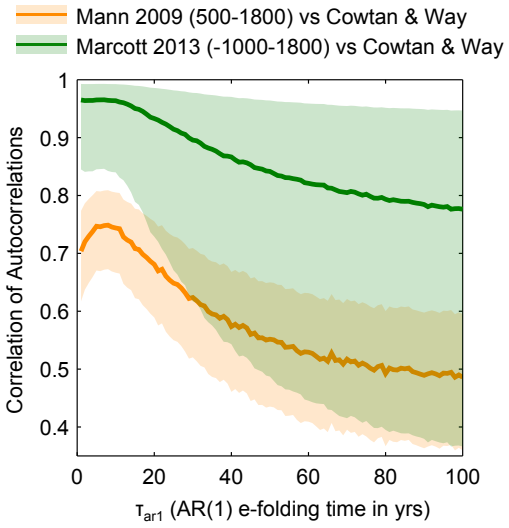

Figure 5.6: **Correlation of the autocorrelations of $S(t)$ and the instrumental record by Cowtan & Way (2014).** Shown here are the full range and median of autocorrelations (y-axis) of 1000 detrended draws of $\mathbf{T}$ up to 1800 CE, with different Ω (x-axis) and the detrended instrumental record by Cowtan & Way (2014). The different colours denote both proxy temperature sets used (Mann *et al.* (2009), Marcott *et al.* (2013)).

For each draw of parameters $\mathbf{\Psi_i}$, i.e. each iteration of the MH algorithm, $n = 100$ samples $\mathbf{T_j}$, given $\mathbf{S}$, are drawn, while $\mathbf{S}$ and $\mathbf{T}$ have uninformative, flat, priors meaning that $P(\mathbf{T}|\mathbf{S}) = P(\mathbf{S}|\mathbf{T})$. From this set of temperatures the

Table 5.4: **Semi-empirical prior and posterior distributions for the parameters $\mathbf{\Psi}$.** $\mathcal{N}(\mu,\ \sigma^2)$ denotes a normal distribution around μ with the standard deviation σ. $U(x_1,\ x_2)$ is a uniform distribution between x_1 and x_2. Ranges shown for posteriors are 90% confidence intervals. Temperatures are given relative to the 1850–2000 CE average.

Parameter	Prior	Mann *et al.* (2009)	Marcott *et al.* (2013)
a	$U(0, 20)$ mm/y/K	$4.0\ (3.2, 5.2)$	$4.0\ (3.1, 5.4)$
c(500 CE)	$U(-10, 10)$ mm/y	$0.22\ (0.07, 0.44)$	$0.05\ (0.02, 0.10)$
c(2000 CE)	$U(-2, 2)$ mm/y	$0.10\ (0.03, 0.28)$	$0.03\ (0.00, 0.08)$
T_0(2000 BCE)	$< T(2000 - 1800 \text{ BCE}) > + U(-0.6, 0.6)$	$0.11\ (0.03, 0.28)$	$0.03\ (0.00, 0.08)$
T_0(500 CE)	$\mathcal{N}(< T(500 - 700 \text{ CE}) >,\ (0.2 \text{ K})^2)$	$0.17\ (0.11, 0.23)$	$-0.09\ (-0.16, -0.02)$
T_0(2000 CE)		$-0.07\ (-0.13, 0.04)$	$-0.03\ (-0.14, 0.09)$
τ	$\log\ U(30, 3000)$ yrs	$204\ (103, 413)$	$147\ (84, 293)$
τ_c	$\log\ U(1000, 20000)$ yrs	$3112\ (1078, 16066)$	$3071\ (1110, 16034)$

semi-empirical sea level $\mathbf{h}_{i,j} = \mathbf{h}(\mathbf{\Psi}_i, \mathbf{T}_j)$ is calculated according to equation 5.2 and compared to GSL $\mathbf{g} \sim \mathcal{N}(\hat{\mathbf{g}}, \mathbf{\Sigma})$. From this comparison the posterior probability distribution $P(\mathbf{\Psi}_i|\mathbf{g}, \mathbf{S})$ is calculated according to equations 5.3 and 5.4.

$$\begin{aligned} P(\mathbf{\Psi}_i|\mathbf{g}, \mathbf{S}) &\sim P(\mathbf{g}|\mathbf{\Psi}_i, \mathbf{S})\ P(\mathbf{\Psi}_i) \\ &\sim P(\mathbf{g}|\mathbf{\Psi}_i, \mathbf{T})\ P(\mathbf{T}|\mathbf{S})\ P(\mathbf{\Psi}_i) \\ &\approx \frac{1}{n}\sum_{j=1}^{n} P(\mathbf{g}|\mathbf{\Psi}_i, \mathbf{T}_j) P(\mathbf{\Psi}_i) \end{aligned} \tag{5.3}$$

$$P(\mathbf{g}|\mathbf{\Psi}_i, \mathbf{T}_j) = |2\pi\mathbf{\Sigma}|^{-1/2} \exp\Big(-\frac{1}{2}[\hat{\mathbf{g}} - \mathbf{h}_{i,j}]^\top \mathbf{\Sigma}^{-1} [\hat{\mathbf{g}} - \mathbf{h}_{i,j}]\Big) \tag{5.4}$$

In equation 5.3, $P(\mathbf{\Psi})$ gives the prior and $P(\mathbf{\Psi}|\mathbf{g}, \mathbf{S})$ the posterior probability distributions, both listed in table 5.4.

In order to tare the models ability to fit GSL and the rate of GSL change the covariance matrix $\mathbf{\Sigma}_r$ resulting from the Gaussian-process model of equation 5.1 gets tapered. The tapered matrix $\mathbf{\Sigma} = \mathbf{\Sigma}_r \circ \lambda$ is the entrywise product of the original matrix $\mathbf{\Sigma}_r$ with the exponentially falling tapering function $\lambda_{i,j} = \exp(-|t_i - t_j|/\tau_{cov})$. The timescale τ_{cov} was chosen to be 100 yrs which is, as shown in figure 5.7, the maximum likelihood value, comparing different values $\tau_{cov} \in \{10, 50, 100, 200, 500, 1000\}$ as well as no tapering ($\tau_{cov} = \infty$) and full tapering, i.e. a diagonal covariance matrix ($\tau_{cov} = 0$).

For calculating the 20th century GSL under the above introduced coun-

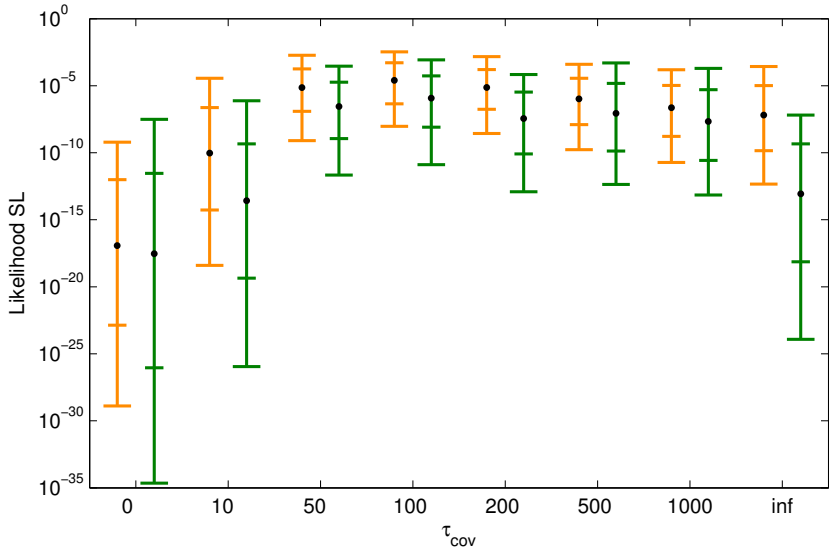

Figure 5.7: **Likelihood $P(\mathbf{\Psi}_i|\mathbf{g},\mathbf{S})$ for different covariance tapering timescales τ_{cov}.** The bars give the 67% and 90% confidence intervals for the likelihood of individual semi-empirical hindcasts $\mathbf{h_{ij}}$ while the black dot gives the likelihood across all hindcasts. The colours symbolize calibrations with both temperature proxies Mann *et al.* (2009) and Marcott *et al.* (2013) (orange and green).

terfactual temperature scenarios ($\mathbf{T}'$), from 1900 CE onwards the term $\mathbf{T}_j$ in equations 5.3 and 5.4 is replaced by $\mathbf{T}'_j$ so that either $\mathbf{T}'_j$ follows the linear rate of $T_j(500 - 1800\text{CE})$ (Scenario 1) or $\mathbf{T}'_j = \langle T_j(500 - 1800\text{CE})\rangle$ (Scenario 2). The factual sea level, i.e. the historic baseline, was calculated by substituting $\mathbf{T}_j$ by the HadCRUT4 instrumental temperature $\mathbf{T}''_j$ after 1900 CE. $\mathbf{T}''_j$ was made to have the same offset as $\mathbf{T}_j$ between 1850–1900 CE while for Scenario 1 $T'_j(1900\text{CE}) = \langle T_j(1801 - 1900\text{CE})\rangle$. Now the anthropogenic and the non-anthropogenic contributions to sea-level change, as listed in table 5.1,are calculated according to $\mathbf{h}(\mathbf{\Psi}_i, \mathbf{T}'_j)/\mathbf{h}(\mathbf{\Psi}_i, \mathbf{T}''_j)$ and $\mathbf{h}(\mathbf{\Psi}_i, \mathbf{T}''_j) - \mathbf{h}(\mathbf{\Psi}_i, \mathbf{T}'_j)$, respectively. The likelihood that at a given time the counterfactual sea-level hindcasts are exceeded by observed GSL rise, as given in table 5.2, is the number of times that $\mathbf{h}(\mathbf{\Psi}_i, \mathbf{T}''_j) - \mathbf{h}(\mathbf{\Psi}_i, \mathbf{T}'_j) > 0$ divided by $m * n$.

For projecting 21st century GSL (figure 5.3d and table 5.3) temperature pathways had been calculated from the RCPs with the simple climate model MAGICC6 (Model for the Assessment of Greenhouse Gas Induced Climate Change, Meinshausen *et al.* (2011)) in probabilistic mode, similar to Schaeffer *et al.* (2012). A Bayesian analysis of historic data sets the input parameter distributions for MAGICC6 (Rogelj *et al.* (2012)) while the climate sensitivity distribution is taken from IPCC (2013). For each RCP 600 temperature realizations of MAGICC6 are combined with every parameter set $\mathbf{\Psi}_i$ and historical temperature $\mathbf{T}_j$. This gives $600 * n * m$ combinations which makes the final uncertainty a combination of parameter, initial condition and projected temperature uncertainty.

Chapter 6

Holocene sea level

The Holocene is the last epoch of the Quaternary period which started ∼2.6 million years ago. The Quaternary is governed by so called Milankovich cycles (Laskar *et al.* (2004)) which cause cyclic growth and decay of continental ice sheets and thus dramatically change the climate conditions. Milankovich cycles are characterized by changes in the so called orbital forcing, i.e. changes of incoming solar radiation resulting from a combination of parameter changes. These parameters are the Earth's rotation axis tilt, eccentricity and precession which mainly change the latitudinal and seasonal dependence of the radiative forcing (IPCC (2007)). The mean global and annual solar insolation is not changed by oscillating orbital parameters, only eccentricity has a minor impact. The reason for the growth of large northern hemisphere ice sheets is the low summer temperature above 65°N which enables ice to persist over summer and thus to grow over winter. The observed global temperature (figure 6.3b) and CO_2 drop during glacial periods must be explained with climate and biophysical feedbacks (IPCC (2007)).

6.1 Temperature and sea-level evolution

The current interglacial period, the Holocene, started around 12,000–7,000 BP (before present, conventionally 1950 CE) (Törnqvist & Hijma (2012)) and is roughly characterized by different episodes. Looking at the global temperature evolution from Marcott *et al.* (2013) in figure 6.1b there was a gradual temperature increase of about 0.6°C between 9300–7500 BCE fol-

lowing the termination of the last glacial period. From there on until about 3500 BCE temperature stabilized on a relatively high level sometimes called 'Holocene Optimum'. After 3500 BCE temperature started its late Holocene, long-term, 0.7°C cooling until the onset of the anthropogenic warming about 1850 CE. This decrease was interrupted by the medieval climate anomaly (MCA, 950–1250 CE) and the little ice age (LIA, 1400–1700 CE) (Mann *et al.* (2009)). According to model estimates, corrected for negative vegetation and dust forcings, global mean surface temperature during the last glacial maximum (LGM, 19–23 ka BP (Before Present)) was 4–7°C lower than pre-industrial (IPCC (2007)). This is in good accordance with model results constrained by proxy data like Schneider von Deimling *et al.* (2006) and Holden *et al.* (2010), giving a best estimate of around 6°C. The model-data synthesis of Annan & Hargreaves (2013) as well as the global proxy-temperature compilation of Shakun *et al.* (2012) represent the lower edge of this range.

The northern hemisphere, main object to the changes in orbital forcing, has a different temperature evolution with higher amplitudes. Greenland ice-sheet reconstructions from Dahl-Jensen *et al.* (1998) show a relatively linear warming of 20.5°C from the LGM to the Holocene climatic optimum and a 2.5°C cooling from then until 1950 CE. From a combination of proxies from four sites Vinther *et al.* (2009) find similar Holocene Greenland temperatures with less pronounced MCA and LIA (see figure6.1a).

Eustatic sea level during glacial-interglacial periods varies mainly due to changing land-ice masses and Earth's dynamic response to the surface loading. The Lambeck *et al.* (2014) global sea-level reconstruction from a combination of approximately 1000 far-field sides (far from former ice margins), complemented by independent near field analysis of the major ice sheets, is shown in figure 6.1c, d and back to the LGM in figure 6.3a. GSL at the LGM was about 130 m below present values. It started to rise, first slowly, then from about 14,500–6,200 BCE more rapidly with an average rate during this deglaciation period of about 1.2 meter per century. During meltwater-pulse 1A (MWP-1A, 12,550–12,050 BCE) the rates even reached up to $\geq$4 meters per century. The further the Holocene proceeded the more the rates of GSL rise decreased until, from 500–1800 CE GSL rise almost stopped (Lam-

beck *et al.* (2014)). Comparing total sea-level rise and its behaviour since the LGM, this comprehensive analysis is in accordance with earlier far-field multi-proxy studies (Fleming *et al.* (1998) and Peltier (2002)) as well as the statistical analysis of Stanford *et al.* (2011). Still they differ in the exact dating and thus also magnitude of certain features like MWP-1A. Stanford *et al.* (2011) define MWP-1A over a period of 1500 years instead of 500 years and thus conclude much lower sea-level rise of only 1.0–1.3 meters per century.

6.2 Semi-empirical approach

GSL rise, although slowing down, occurs despite of the long-term Holocene cooling, giving a good example of the high inertia of sea-level change. This invokes the question whether the semi-empirical principle, namely $\mathrm{d}h/\mathrm{d}t \propto T$, is applicable on Holocene time scales. One immediate problem for the semi-empirical models is the forcing on these time scales. Contrary to the present-day global greenhouse-gas forcing which changes global temperature, the orbital forcing, as mentioned above, has almost no global impact. It is the local differences in forcing and the resulting feedbacks that let sea level rise during the termination of the last glacial and into the Holocene. This problem might in parts be resolved when disentangling the contributions to the Holocene sea-level rise. Unfortunately, the data for the southern hemisphere is very sparse. One data-constrained large ensemble analysis of Antarctica by Briggs *et al.* (2014) gives an average rate of approximately 0.07 cm/yr from -10,000–1950 CE and around 0.14 cm/yr from 10,000–6,000 BCE, a period for which Golledge *et al.* (2014) find an ensemble mean rate of $\sim$0.1 cm/yr. Given the Holocene amplitude of global temperature change of about 0.7°C, this would cause a thermosteric equilibrium sea-level change of only about 0.3 m according to Levermann *et al.* (2013), who found the linear relationship of 0.42 m/K. These are comparatively small contributions given the global Holocene rise of about 60 m as can be seen in figures 6.1c and d. The main sea-level contribution was thus delivered by northern-hemisphere ice, which is to be expected from the nature of Milankovich forcing and the continental geometry. Holocene sea level might hence be semi-empirically understood, if assumed to be driven by a single component. Slightly chang-

ing the semi-empirical principle ($\mathrm{d}h/\mathrm{d}t \propto T_{\mathrm{NH}}$), might thus be adequate to model Holocene sea level semi-empirically. This is basically analogous to the approach of Vermeer & Rahmstorf (2009) who modelled thermal expansion, and to the attempt of chapter 3 to model glacier and ice caps. It will be shown that this approximation alone does not resolve the problem of a rising GSL with simultaneously dropping temperatures and that a long term trend, possibly from Antarctica, is inescapable.

PALSEA (2010) discuss three characteristic patterns of sea-level response to temperature change during the termination of the last glacial. An exponential, a linear and an asymptotic one (the latter one is shown in figure 1.3). PALSEA (2010) are able to exclude the exponential response with paleo-data constraints. Based on this, in the following, two semi-empirical models will be tested on their ability to capture Holocene sea level from around 10,000 BCE to 1800 CE. The first model, henceforth called 'simple', is similar to equation 1.1 from Rahmstorf (2007), except that the equilibrium temperature T_0 decays on the time scale τ (equation 6.1). It resembles the asymptotic response proposed by PALSEA (2010). The second model is supplemented with an additional constant rate c and will be called 'constant rate' (equation 6.2). This model is thus a combination of linear and asymptotic response with the limitation that the linear part is constant and not temperature dependent.

$$\mathrm{d}h/\mathrm{d}t = a\,(T - T_0) \tag{6.1}$$

$$\mathrm{d}h/\mathrm{d}t = c + a\,(T - T_0) \tag{6.2}$$

$$\mathrm{d}T_0/\mathrm{d}t = (T - T_0)/\tau \tag{6.3}$$

The posterior parameter distributions which are plotted in figure 6.2 and listed in table 6.1 were evaluated by a Metropolis-Hastings algorithm as explained in the methods section 6.4. Two temperature data sets will be tested to fit the sea-level reconstruction of Lambeck *et al.* (2014): the global RegEM temperature reconstruction by Marcott *et al.* (2013) (MAR) which was also used in previous chapters and the mean Agassiz and Renland δ^{18}O Greenland temperature reconstruction, corrected for surface-elevation changes, from Vinther *et al.* (2009) (VIN) as a representation of high latitude northern

hemisphere temperature. The two sites Agassiz and Renland have the advantage of not being influenced by ice flow and having an elevation history that can be reconstructed with some confidence. Uplift-corrected temperatures from both sites are very similar despite of the sites being 1500 km apart and divided by the entire Greenland ice sheet. Vinther *et al.* (2009) thus conclude that Holocene climate in Greenland was relatively homogeneous and is well represented by the mean temperatures from Agassiz and Renland. As explained above, northern hemisphere temperatures are expected to be more suited as model drivers. However, this assumption needs to be evaluated against global temperature.

It was not possible to find a parameter set with a probability >0 for the simple model and the VIN temperature. This is probably due to the shorter duration of the climatic optimum as compared to MAR. The VIN temperature starts its long-term Holocene fall earlier than MAR, what makes the falling-temperature-rising-sea-level discrepancy even more difficult to describe. In figures 6.1c, 6.2c, f and g calibrations with both models and the MAR temperature are compared. Clearly, the simple model performs worst. In order to cope with falling temperature and rising sea level long time scales τ and small sensitivities a are selected. This way the reversal from sea level rise to fall in the model is postponed to around -1360 CE. But the low sensitivity only allows for about half of the early Holocene sea-level rise to be modelled.

A constant rate seems necessary to find a meaningful calibration over the whole Holocene. To test whether this is owed to either the fast increasing sea level during the early Holocene or the slowly rising sea level with simultaneously falling temperatures in the later Holocene, the data can be divided roughly in the middle of the climatic optimum into in two periods, from 10,000–5000 BCE and 5000 BCE to 1800 CE. Calibrating both models, driven by both temperatures, to both periods, it turns out that for none of the combinations a constant rate is necessary. This means that it is the combination of sea-level behaviours in the early and late Holocene that makes the constant rate necessary.

Comparing the calibrations with the constant rate model and both temperatures as done in figures 6.1d and 6.2, the VIN temperature seems to be suited better. Only by selecting extremely low initial equilibrium temper-

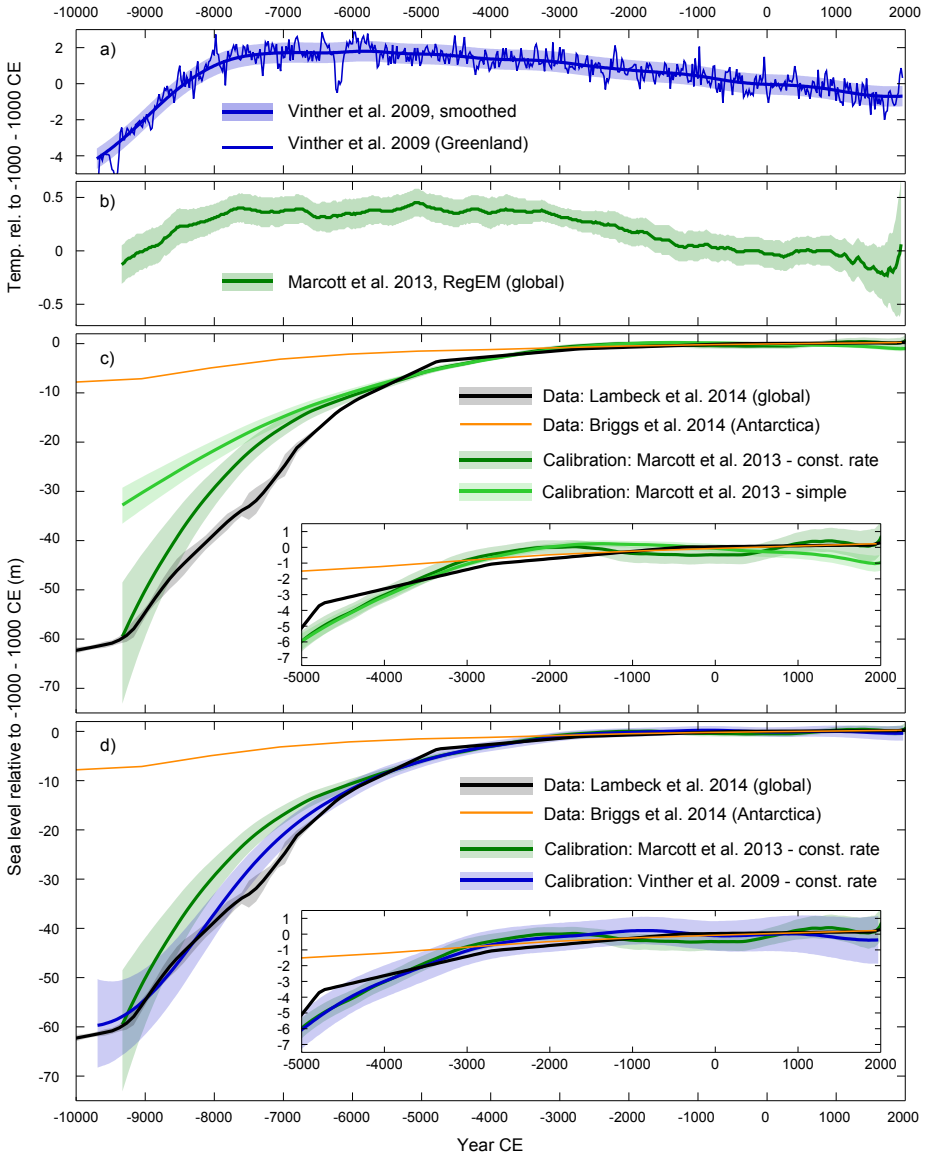

Figure 6.1: **Semi-empirical calibrations of Holocene sea level with global and Greenland temperatures.** (a) Vinther *et al.* (2009) Greenland temperatures un-smoothed and smoothed with one standard deviation evaluated from the residual of both. (b) Marcott *et al.* (2013) global RegEM reconstruction with one standard deviation. (c)-(d) Semi-empirical calibrations with the above temperatures and two models (equations 6.1 & 6.2) to the Lambeck *et al.* (2014) global sea-level. For comparison the Briggs *et al.* (2014) Antarctic sea-level contribution from their figure 13 is shown in orange. The data uncertainty is one sigma while the calibrations are 90% confidence intervals. All data is given with respect to the mean of -1000–1000 CE.

Table 6.1: **Semi-empirical posterior distributions for the parameters Ψ.** Ranges shown for posteriors are 90% credibility intervals. Temperatures are given relative to the -1000–1000 CE average.

	Vinther *et al.* (2009) constant-rate model		Marcott *et al.* (2013) constant-rate model		Marcott *et al.* (2013) simple model	
Ψ	50%	5–95%	50%	5–95%	50%	5–95%
a (cm/yr/K)	0.62	(0.46, 0.92)	1.67	(1.17, 2.66)	0.48	(0.42, 0.55)
c (cm/yr)	0.27	(0.21, 0.34)	0.19	(0.15, 0.25)	–	–
τ (yrs)	1219	(929, 1497)	1294	(941, 1612)	3389	(3167, 3657)
$T_0(1^{\text{st}}$ yr) (°C)	-4.76	(-6.07, -3.01)	-1.87	(-2.01, -1.26)	-1.94	(-2.03, -1.67)

atures can the early Holocene sea-level rise be accounted for in the MAR simulation, but with bigger deviations than with the VIN temperature. This low initial T_0 seems unrealistic as the reality check in figure 6.3b reveals.

It is safe to assume that the sea level was in equilibrium at the LGM, naturally resulting in a lower limit for $T_0(\text{LGM})$, which is $T_0(\text{LGM}) \approx T(\text{LGM})$. The lower-limit assumption is justified because sea level was falling until the LGM and thus $T_0(\text{LGM}) > T(\text{LGM})$. With the calculated τ_{MAR} and the best estimate of global temperature from Shakun *et al.* (2012), T_0 (equation 6.3) can be calculated for the termination of the last glacial (figure 6.3b). Although T_0 needs to be considered a lower limit, it turns out that at the beginning of the MAR temperature series it is considerably higher than the one selected by the model. So if the prior distributions, which were flat for these simulations, were set accordingly, or the model would have a spin up, the calibrations with the MAR temperature would probably turn out worse. Yet a spin up with a single temperature reconstruction is not advisable because, as mentioned above, the amount of LGM cooling is confined only to a range of a few degrees Celsius.

Forcing the semi-empirical constant-rate model with the Greenland temperatures by Vinther *et al.* (2009), realistic values for the initial T_0 are selected. The full posterior parameter distributions are plotted in figure 6.2 and listed in table 6.1. The selected sea-level sensitivity is higher than the one found for the last 3000 years in chapter 5 but with overlapping uncertainties (i.e. 6.2 (4.6, 9.2) as compared to 4.0 (3.1, 5.4) mm/yr/K, 90% CI). Both τ and c are about one order of magnitude higher than for calibrations of the last 3000 years. This is not surprising because the latitudinal signature of the forcing as well as the processes governing sea-level change are very

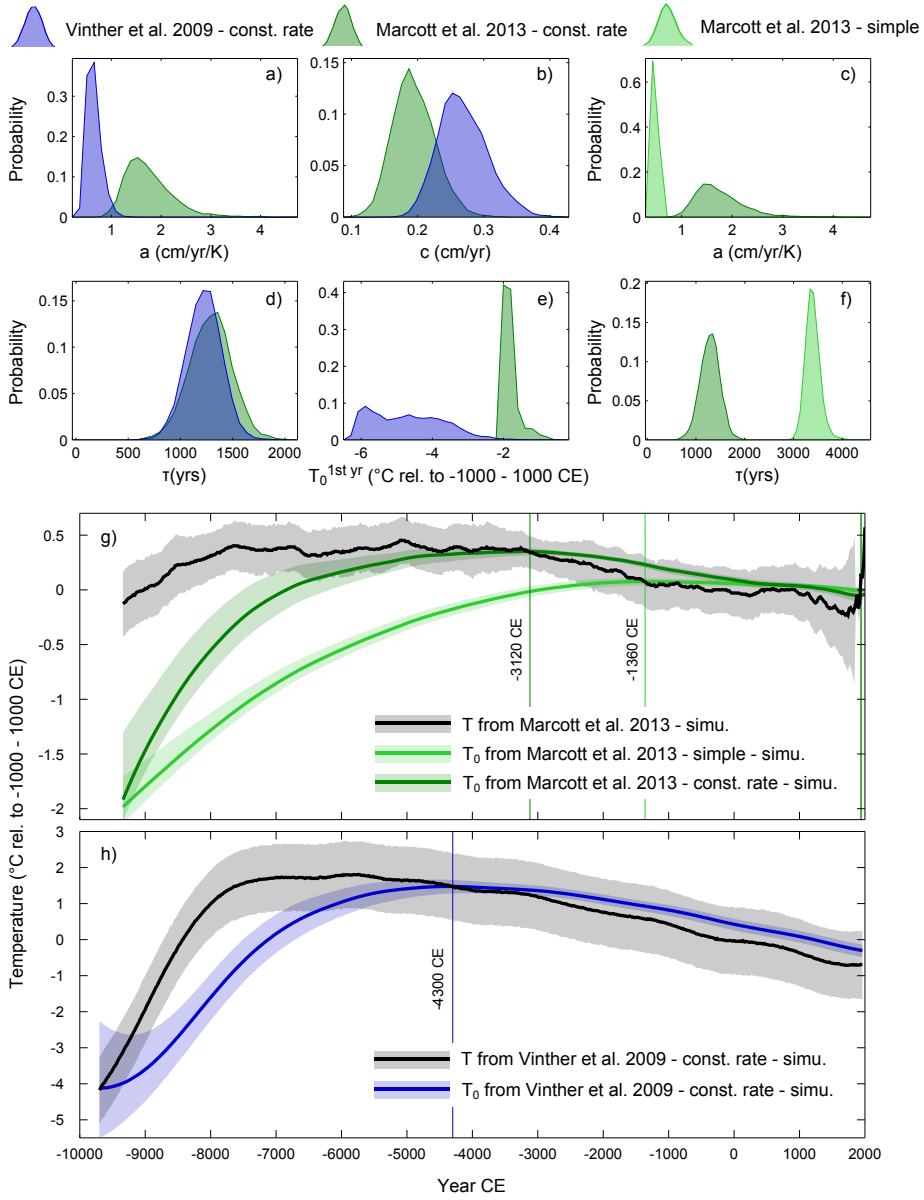

Figure 6.2: **Posterior parameter distributions for Holocene sea-level simulations.** (a)-(f) Full posterior parameter distributions for the simulations described in the text. The binning for all histograms is 30 except for (f) where 66 bins was used so the probability is the same as in (d). (g)-(f) The evolution of $T_0(t)$ (green and blue) plotted with the driving simulated temperatures $T(t)$ (grey). Both semi-empirical models from equations 6.1 & 6.2 and calibration temperatures are compared. The vertical lines give the year that T_0 cuts T. All confidence intervals are 90 %.

different in the early and late Holocene, including the industrial era. For this reason the above model was only calibrated until 1800 CE, excluding the recent global warming. Yet both periods can be looked upon semi-empirically without contradiction. Northern hemisphere land-ice changes, as mentioned above, are the main contributors to sea-level change during deglaciation and the early Holocene. But the necessity of an additional constant rate points to a long term rise with a timescale $\gg \tau$. The most likely source for this long term rise is the Antarctic and indeed the above mentioned Antarctic sea-level contribution from Briggs *et al.* (2014) (0.14 cm/yr from 10,000–6,000 BCE) and Golledge *et al.* (2014) ($\sim$0.1 cm/yr from 10,000–6,000 BCE) are of the same order of magnitude, although smaller, than the selected constant rate (0.21–0.34 cm/yr, 90% CI). The difference in size might be caused by an incomplete semi-empirical model that either misses a certain process, contributing positive to sea-level change, or wrongfully takes the Antarctic contribution to be constant. It might also be the case that Greenland temperature, as forcing, is not the optimal choice, maybe giving too much weight to high latitudes. Besides the exact size of the constant rate, attributed to Antarctica, it is interesting to see that it is positive and greater zero. This contradicts a study by Zwally *et al.* (2015) who find that Antarctica as a whole is currently contributing negative to sea-level change as a consequence of a mass accumulation increase in East Antarctica that started 10,000 years ago. In the semi-empirical model both hemispheres contributed to sea-level rise from the LGM to the Holocene climatic optimum (in this model until about 4300 BCE as shown in figure 6.2h). From there on it was a combination of contrary trends, a sea-level fall due to falling temperatures and a positive contribution owed to the high inertia of sea level. The high inertia is a consequence of the long memory of ice-sheets which can well contribute to sea level rise long after climate stabilized. The temperature induced sea-level fall should be caused by land-ice accumulation and to a minor extent by thermosteric sea-level change.

6.3 Conclusions

Holocene eustatic sea level from about -10,000–1800 CE is characterized by an increase of about 60 m which is constantly slowing down until it almost stabilizes between 500–1800 CE. To semi-empirically capture this behaviour it is necessary to employ a model with one temperature dependent term supplemented by a constant rate. It was found that, due to the nature of orbital forcing, northern-hemisphere (in this case Greenland, VIN) temperature performs best as model driver. This is owed to the fact that it can capture northern-hemisphere land-ice changes which are expected to play the dominant role in the Holocene sea-level history. The adjustment timescale for this contribution is 1219 (929–1497) years (90% confidence). The inescapable constant rate turns out to be of the same order of magnitude as reconstructions of Antarctic sea-level contributions. In reality this contribution is not constant but probably has a dominant timescale which is large compared to the time considered. In order to attribute sea-level change more precisely to certain contributors better data would be necessary especially for Antarctica. Then a separate model could be calibrated to this contribution which is now reduced to one rate.

6.4 Methods

The semi-empirical models given in equations 6.1 & 6.2 are calibrated similar to chapter 5 and described in the methods section 5.4 with a few differences. A Metropolis-Hastings (MH) algorithm (Hastings (1970)) is used to sample from the posterior distribution $P(\mathbf{\Psi}|g(t), T(t))$ of the parameters $\mathbf{\Psi} = \{a, c, \tau, T_0(t)\}$ (equations 5.3 & 5.4). The starting parameter set is evaluated via simulated annealing. The first 1000 samples are discarded in a so called burning-in period and the Markov chain is then thinned to every 1000th sample to eliminate autocorrelation in the posterior samples. The final sample size is $m = 1000$. The parameter prior distributions $P(\mathbf{\Psi})$ are chosen to be flat, i.e. constant, not constraining the posterior in equation 5.3.

The two temperature proxy datasets $S(t)$ used are the global Marcott

et al. (2013) RegEM data (MAR) and the Greenland data from Vinther *et al.* (2009) (VIN). The MAR data was treated as described in chapter 5.4. Supplementing the MAR temperature with 20-year average values of the HadCRUT3 instrumental data (Brohan *et al.* (2006)) does not matter here because the calibration period ends 1800 CE. The VIN temperature was modelled as an AR(1) process with the smoothed VIN temperature as expectation value $S(t)$ (equation 4.1). The correlation coefficient was determined with the Yule-Walker equation from the residual of the smoothed and unsmoothed VIN temperatures (figure 6.1a).

The Lambeck *et al.* (2014) global sea level data, which is the calibration target, is only published with standard errors and without covariances. To account for autocorrelations, the data get downweighted by inflating the uncertainties by a factor of 10 (Kemp *et al.* (2011)).

The Briggs *et al.* (2014) data from figures 6.1c and d was obtained from their figure 13 by digitizing it graphically only to give a qualitative comparison to global sea level.

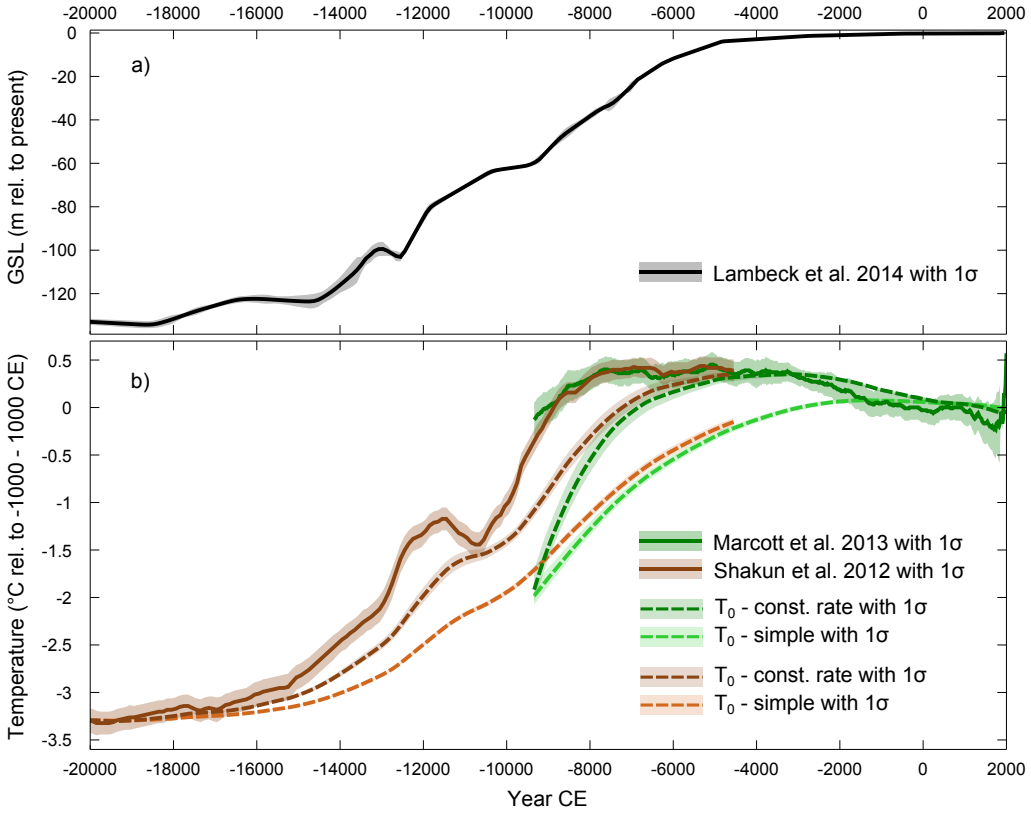

Figure 6.3: **GSL, temperature, and equilibrium temperature T_0 from the LGM to present.** (a) Lambeck *et al.* (2014) sea level with one sigma uncertainty relative to present (1950 CE). (b) Solid lines show Marcott *et al.* (2013) RegEM (MAR) and Shakun *et al.* (2012) (SHA) temperatures. MAR is given relative to -1000–1000 CE while SHA is levelled to the MAR data over their period of overlap. The dashed dark/light green curves show T_0 from figure 6.2g corresponding to model equations 6.2 and 6.1, respectively. The dashed dark/light brown curves give T_0 calculated with the timescales of the dark/light green curves and driven by the best estimate SHA temperature assuming that $T_{\mathrm{SHA}}(20,000\ \mathrm{BCE}) = T_0(20,000\ \mathrm{BCE})$.

Chapter 7

Final words

7.1 Summary

On the preceding pages different aspects of global sea-level change have been semi-empirically examined. Semi-empirical models have been validated, used on the sea-level contribution of glaciers, and to infer global temperature from sea level. Periods studied encompass the instrumental period with tide gauges (starting 1700 CE in Amsterdam) and satellites (first launched in 1992 CE), the Common Era from -1000 CE onwards, and the full length of the Holocene since about 10,000 BCE. Accordingly different data, model formulations and implementations have been used.

Chapter 2 demonstrated the predictive skills of different semi-empirical models. Using a combination of tide-gauge and proxy sea-level data for calibration, a 20th century sea-level rise of 13–30 cm (90% confidence range) is predicted while the observed interval from two, tide-gauge based, GSL data sets is 14–26 cm. Comparing the predictive skill for the period 1961–2003 CE to that of process-based models published in the IPCC (2007) AR4, it turned out that semi-empirical models, although dependent on the right data use, were indeed superior. This analysis sparked an effort to review the predictive skills also of state-of-the-art process-based models by Church *et al.* (2013) which had a big influence on the IPCC (2013) AR5.

In chapter 3 an attempt was started to model a single component of sea-level change, namely the glacier and ice cap contribution as simulated by Radić & Hock (2011). This study failed to give a consistent picture. The pro-

posed most likely reason is a shortcoming of the used data although model insufficiencies can not fully be ruled out. In this case the semi-empirical model was still helpful in disclosing data issues. Hence, it could be shown that neglecting parts of the data improved the simulations considerably, giving another hint to possible initialization issues. Based on the data of Radić & Hock (2011) the semi-empirical model predicts that glaciers and ice caps would not have been stable in the pre-industrial climate. This counterfactual result is also a strong hint towards flawed data.

To resolve problems of previous publications, when calibrating a semi-empirical model to data from before 1100 CE, chapter 4 introduced a better uncertainty representation of the driving temperature. It was found that the semi-empirical connection between sea level and temperature indeed holds true also prior to 1100 CE. By inverting the simulation chain and inferring temperature from sea level it could be shown that a temperature step around 1100 CE, present in the reconstruction of Mann *et al.* (2008) and troubling previous semi-empirical models, is most likely (>90% confidence) artificial.

To calibrate a semi-empirical model over the Common Era for determining anthropogenic contributions and updating projections, a newly compiled global sea-level reconstruction was used in chapter 5. This is the first time a semi-empirical model was used with a truly global compilation of sea-level proxy data. Using two long-term global temperature reconstructions for calibration, the model could fit GSL well. New projections until 2100 CE largely reconcile the differences between semi-empirical and process-based models published in the AR5 IPCC (2013). With these new calibrations it also showed to be extremely likely ($P = 0.95$) that more than 40 % of the observed global sea-level rise in the 20th century is owed to human-induced global warming, which is in accordance with literature.

Finally, in chapter 6, the attention was turned to the Holocene sea level in its full length. To semi-empirically cope with this it could be shown that northern hemisphere (in this case Greenland) temperatures serve as a good driver, superior to global temperatures. This is a consequence of the nature of Milankovich forcing which is the main driver on Holocene timescales. To conciliate a constantly rising sea level with temperatures that peak during the Holocene climatic optimum, a semi-empirical model with a constant rate is

favourable. The resulting simulated sea level is thus a linear combination of a temperature dependent term, accounting for northern hemisphere land-ice changes, and a constant rate. Both turn out to contribute positive to sea-level change until sometime during the climatic optimum from where on the temperature dependent term causes sea level to fall while the constant rate still contributes positive. The constant rate is of the same order of magnitude as reconstructions of the Antarctic Holocene sea-level contribution. Sea level in the second half of the Holocene (from about 4300 BCE onward) is thus found to be governed by a falling component from the northern and a rising component from the southern hemisphere.

7.2 Outlook

By now semi-empirical models of global sea-level change (SEMs) have a history of more than 8 years of extensive research and number among the most cited sea-level publications. In the beginning they mainly aimed at disclosing unrealistically low projections by process-based models which they have done tremendously successfully. Meanwhile they were used, tested and improved in numerous ways. To a large extent the projection discrepancies of process-based and semi-empirical models vanished because of improvements from both sides. But still SEMs are not outdated because they retain their big advantage of being simple and fast. The simplicity still makes it possible to explore fundamental issues, like the Holocene sea level, because the setting up of simulations as well as the interpretation of results is comparatively easy. The fast computation, on the other hand, makes SEMs a good tool for assessments. While process-based models usually only project sea level for the IPCC scenarios, SEMs can be easily used to compare different alternatives of, for example, greenhouse gas mitigation or to calculate certain contributions, like the anthropogenic one. It can thus be expected that SEMs will in future have a big impact in the assessment literature while continuing to play an important role in basic science.

Abbreviations

A1B high emissions scenario (IPCC (2000))

AOGCM Atmosphere Ocean General Circulation Model

AR(1) Auto-regressive process of order one

AR4/5 Assessment Report 4/5 by the IPCC

BCE Before the Common Era

BP Before Present (1950 CE)

CE Common Era

CPS Composite Plus Scale

CW11 sea-level data of Church & White (2011)

EIV Error In Variables

GIA Glacial-Isostatic Adjustment

GIC Glaciers and Ice Caps

GISS Goddard Institute for Space Studies

GSL Global Sea Level

HadCRUT Temperature record compiled by the Hadley Centre and the Climatic Research Unit (Brohan *et al.* (2006))

IPCC Intergovernmental Panel on Climate Change

JE08 sea-level data of Jevrejeva *et al.* (2008)

KE11 sea-level data of Kemp *et al.* (2011)

LGM Last Glacial Maximum

LIA Little Ice Age

MAGICC Model for the Assessment of Greenhouse Gas Induced Climate Change

MAR temperature data from Marcott *et al.* (2013)

MCA Medieval Climate Anomaly

MH Metropolis-Hastings (Hastings (1970))

MN08 temperature data from Mann *et al.* (2008)

MWP Melt Water Pulse

NH Northern Hemisphere

PALSEA Paleo Sea level working group

RCP Relative Concentration Pathway (Van Vuuren *et al.* (2011))

RegEM Regularized Expectation Maximization

RegEM CFR RegEM Climate Field Reconstruction

RH GIC data of Radić & Hock (2011)

RSL Relative Sea Level

RT model introduced by Rahmstorf (2007)

SEM Semi-Empirical Model

SHA temperature data from Shakun *et al.* (2012)

SL Sea Level

ssa singular spectrum analysis

VIN temperature data from Vinther *et al.* (2009)

VR model introduced by Vermeer & Rahmstorf (2009)

Bibliography

Ahmed, M., et al. 2013. Continental-scale temperature variability during the past two millennia. *Nature geoscience*, **6**(5), 339–346.

Alley, R.B., & Joughin, I. 2012. Modeling Ice-Sheet Flow. *Science*, **336**(6081), 551–552.

Annan, J.D., & Hargreaves, J.C. 2013. A new global reconstruction of temperature changes at the Last Glacial Maximum. *Climate of the past*, **9**(1), 367–376.

Antonov, J.I. 2002. Steric sea level variations during 1957-1994: Importance of salinity. *Journal of geophysical research*, **107**(C12).

Becker, M., Karpytchev, M., & Lennartz-Sassinek, S. 2014. Long-term sea level trends: Natural or anthropogenic? *Geophysical research letters*, **41**(15), 5571–5580.

Bittermann, K., Rahmstorf, S., Perrette, M., & Vermeer, M. 2013. Predictability of twentieth century sea-level rise from past data. *Environmental research letters*, **8**(1), 014013.

Briggs, R.D., Pollard, D., & Tarasov, L. 2014. A data-constrained large ensemble analysis of Antarctic evolution since the Eemian. *Quaternary science reviews*, **103**, 91–115.

Brohan, P., Kennedy, J.J., Harris, I., Tett, S.F.B., & Jones, P.D. 2006. Uncertainty estimates in regional and global observed temperature changes: A new data set from 1850. *Journal of geophysical research*, **111**(D12).

Chao, B.F., Wu, Y.H., & Li, Y.S. 2008. Impact of artificial reservoir water impoundment on global sea level. *Science*, **320**(5873), 212–214.

Chen, J.L., Wilson, C.R., & Tapley, B.D. 2013. Contribution of ice sheet and mountain glacier melt to recent sea level rise. *Nature geoscience*, **6**(7), 549–552.

Church, J.A., & White, N.J. 2006. A 20th century acceleration in global sea-level rise. *Geophysical research letters*, **33**(1).

Church, J.A., & White, N.J. 2011. Sea-Level Rise from the Late 19th to the Early 21st Century. *Surveys in geophysics*, **32**(4-5), 585–602.

Church, J.A., White, N.J., Konikow, L.F., Domingues, C.M., Cogley, J.G., Rignot, E., Gregory, J.M., van den Broeke, M.R., Monaghan, A.J., & Velicogna, I. 2011a. Revisiting the Earth's sea-level and energy budgets from 1961 to 2008. *Geophysical research letters*, **38**(18).

Church, J.A., Gregory, J.M., White, N.J., Platten, S.M., & Mitrovica, J.X. 2011b. Understanding and projecting sea level change. *Oceanography*, **24**(2), 130–143.

Church, J.A., Monselesan, D., Gregory, J.M., & Marzeion, B. 2013. Evaluating the ability of process based models to project sea-level change. *Environmental research letters*, **8**(1), 014051.

Clark, P.U., Church, J.A., Gregory, J.M., & Payne, A.J. 2015. Recent Progress in Understanding and Projecting Regional and Global Mean Sea Level Change. *Current climate change reports*, **1**(4), 224–246.

Cowtan, K., & Way, R.G. 2014. Coverage bias in the HadCRUT4 temperature series and its impact on recent temperature trends. *Quarterly journal of the royal meteorological society*, **140**(683), 1935–1944.

Dahl-Jensen, D., Mosegaard, K., Gundestrup, N., Clow, G.D., Johnsen, S.J., Hansen, A.W., & Balling, N. 1998. Past Temperatures Directly from the Greenland Ice Sheet. *Science*, **282**(5387), 268–271.

Dangendorf, S., Marcos, M., Müller, A., Zorita, E., Riva, R., Berk, K., & Jensen, J. 2015. Detecting anthropogenic footprints in sea level rise. *Nature communications*, **6**, 7849.

Feulner, G., Rahmstorf, S., Levermann, A., & Volkwardt, S. 2013. On the Origin of the Surface Air Temperature Difference between the Hemispheres in Earth's Present-Day Climate. *Journal of climate*, **26**(18), 7136–7150.

Fleming, K., Johnston, P., Zwartz, D., Yokoyama, Y., Lambeck, K., & Chappell, J. 1998. Refining the eustatic sea-level curve since the Last Glacial Maximum using far- and intermediate-field sites. *Earth and planetary science letters*, **163**(1-4), 327–342.

Foster, G., & Rahmstorf, S. 2011. Global temperature evolution 1979–2010. *Environmental research letters*, **6**(4), 044022.

Foster, G.L., & Rohling, E.J. 2013. Relationship between sea level and climate forcing by CO2 on geological timescales. *Proceedings of the national academy of sciences*, **110**(4), 1209–1214.

Golledge, N.R., Menviel, L., Carter, L., Fogwill, C.J., England, M.H., Cortese, G., & Levy, R.H. 2014. Antarctic contribution to meltwater pulse 1A from reduced Southern Ocean overturning. *Nature communications*, **5**, 5107.

Goosse, H., Crespin, E., Dubinkina, S., Loutre, M.-F., Mann, M. E., Renssen, H., Sallaz-Damaz, Y., & Shindell, D. 2012. The role of forcing and internal dynamics in explaining the "Medieval Climate Anomaly". *Climate dynamics*, **39**(12), 2847–2866.

Gornitz, V., Lebedev, S., & Hansen, J. 1982. Global sea level trend in the past century. *Science*, **215**(4540), 1611–1614.

Gregory, J.M., & Huybrechts, P. 2006. Ice-sheet contributions to future sea-level change. *Philosophical transactions of the royal society a: Mathematical, physical and engineering sciences*, **364**(1844), 1709–1732.

Grinsted, A., Moore, J.C., & Jevrejeva, S. 2009. Reconstructing sea level from paleo and projected temperatures 200 to 2100 AD. *Climate dynamics*, **34**(4), 461–472.

Hansen, J., Ruedy, R., Sato, M., & Lo, K. 2010a. Global surface temperature change. *Reviews of geophysics*, **48**(4).

Hansen, J., Ruedy, R., Sato, M., & Lo, K. 2010b. Global surface temperature change. *Reviews of geophysics*, **48**(4).

Hastings, W.K. 1970. Monte Carlo Sampling Methods Using Markov Chains and Their Applications. *Biometrika*, **57**(1), 97–109.

Hay, C.C., Morrow, E., Kopp, R.E., & Mitrovica, J.X. 2015. Probabilistic reanalysis of twentieth-century sea-level rise. *Nature*, **517**(7535), 481–484.

Holden, P.B., Edwards, N.R., Oliver, K.I.C., Lenton, T.M., & Wilkinson, R.D. 2010. A probabilistic calibration of climate sensitivity and terrestrial carbon change in GENIE-1. *Climate dynamics*, **35**(5), 785–806.

Horton, B.P., Rahmstorf, S., Engelhart, S.E., & Kemp, A.C. 2014. Expert assessment of sea-level rise by AD 2100 and AD 2300. *Quaternary science reviews*, **84**, 1–6.

IPCC. 1990. *Report prepared for Intergovernmental Panel on Climate Change by Working Group I*. Cambridge, Great Britain, New York, NY, USA and Melbourne, Australia: Cambridge University Press.

IPCC. 2000. *Special Report on Emissions Scenarios*. Cambridge, United Kingdom and New York, NY, USA: Cambridge University Press.

IPCC. 2007. *Climate Change 2007: The Physical Science Basis. Contribution of Working Group I to the Fourth Assessment Report of the Intergovernmental Panel on Climate Change*. Cambridge, United Kingdom: Cambridge University Press.

IPCC. 2013. *Climate Change 2013: The Physical Science Basis. Contribution of Working Group I to the Fifth Assessment Report of the Intergovernmental Panel on Climate Change*. Cambridge, United Kingdom and New York, NY, USA: Cambridge University Press.

Jevrejeva, S., & Moore, J. C. 2009. Anthropogenic forcing dominates sea level rise since 1850. *Geophyical research letters*, **36**(20), n/a–n/a.

Jevrejeva, S., Moore, J.C., Grinsted, A., & Woodworth, P.L. 2008. Recent global sea level acceleration started over 200 years ago? *Geophysical research letters*, **35**(8).

Jevrejeva, S., Grinsted, A., & Moore, J.C. 2014. Upper limit for sea level projections by 2100. *Environmental research letters*, **9**(10), 104008.

Joughin, I., Smith, B.E., & Medley, B. 2014. Marine ice sheet collapse potentially under way for the Thwaites Glacier Basin, West Antarctica. *Science*, **344**(6185), 735–738.

Kaser, G., Großhauser, M., & Marzeion, B. 2010. Contribution potential of glaciers to water availability in different climate regimes. *Proceedings of the national academy of sciences*, **107**(47), 20223–20227.

Kemp, A.C., Horton, B.P., Donnelly, J.P., Mann, M.E., Vermeer, M., & Rahmstorf, S. 2011. Climate related sea-level variations over the past two millennia. *Proceedings of the national academy of sciences*, **108**(27), 11017–11022.

Kemp, A.C., Horton, B.P., Vane, C.H., Bernhardt, C.E., Corbett, D.R., Engelhart, S.E., Anisfeld, S.C., Parnell, A.C., & Cahill, N. 2013. Sea-level change during the last 2500 years in New Jersey, USA. *Quaternary science reviews*, **81**, 90–104.

Kemp, A.C., Bernhardt, C.E., Horton, B.P., Kopp, R.E., Vane, C.H., Peltier, W.R., Hawkes, A.D., Donnelly, J.P., Parnell, A.C., & Cahill, N. 2014. Late Holocene sea- and land-level change on the U.S. southeastern Atlantic coast. *Marine geology*, **357**, 90–100.

Konikow, L.F. 2011. Contribution of global groundwater depletion since 1900 to sea-level rise. *Geophysical research letters*, **38**(17).

Kopp, R.E., Horton, R.M., Little, C.M., Mitrovica, J.X., Oppenheimer, M., Rasmussen, D.J., Strauss, B.H., & Tebaldi, C. 2014. Probabilistic 21st and 22nd century sea-level projections at a global network of tide gauge sites. *Earth's future*, **2**(8), 383–406.

Kopp, R.E., Hay, C.C., Little, C.M., & Mitrovica, J.X. 2015. Geographic Variability of Sea-Level Change. *Current climate change reports*, **1**(3), 192–204.

Kopp, R.E., Kemp, A.C., Bittermann, K., Horton, B.P., Donnelly, J.P., Gehrels, W.R., Hay, C.C., Mitrovica, J.X., Morrow, E.D., & Rahmstorf, S. 2016.

Temperature-driven global sea-level variability in the common era. *Proceedings of the national academy of sciences*, **113**(11), E1434–E1441.

Lambeck, K., Rouby, H., Purcell, A., Sun, Y., & Sambridge, M. 2014. Sea level and global ice volumes from the Last Glacial Maximum to the Holocene. *Proceedings of the national academy of sciences*, **111**(43), 15296–15303.

Laskar, J., Robutel, P., Joutel, F., Gastineau, M., Correia, A.C.M., & Levrard, B. 2004. A long-term numerical solution for the insolation quantities of the Earth. *A&A*, **428**(1), 261–285.

Levermann, A., Clark, P.U., Marzeion, B., Milne, G.A., Pollard, D., Radic, V., & Robinson, A. 2013. The multimillennial sea-level commitment of global warming. *Proceedings of the national academy of sciences*, **110**(34), 13745–13750.

Lichter, M., Vafeidis, A.T., Nicholls, R.J., & Kaiser, G. 2011. Exploring Data-Related Uncertainties in Analyses of Land Area and Population in the "Low-Elevation Coastal Zone" (LECZ). *Journal of coastal research*, 757–768.

Little, C.M., Horton, R.M., Kopp, R.E., Oppenheimer, M., Vecchi, G.A., & Villarini, G. 2015. Joint projections of US East Coast sea level and storm surge. *Nature climate change*, **advance online publication**.

Lovelock, C.E., Cahoon, D.R., Friess, D.A., Guntenspergen, G.R., Krauss, K.W., Reef, R., Rogers, K., Saunders, M.L., Sidik, F., Swales, A., Saintilan, N., Thuyen, L.X., & Triet, T. 2015. The vulnerability of Indo-Pacific mangrove forests to sea-level rise. *Nature*, **526**(7574), 559–563.

Mann, M.E., Zhang, Z., Hughes, M.K., Bradley, R.S., Miller, S.K., Rutherford, S., & Ni, F. 2008. Proxy-based reconstructions of hemispheric and global surface temperature variations over the past two millennia. *Proceedings of the national academy of sciences*, **105**(36), 13252–13257.

Mann, M.E., Zhang, Z., Rutherford, S., Bradley, R.S., Hughes, M.K., Shindell, D., Ammann, C., Faluvegi, G., & Ni, F. 2009. Global Signatures and Dynamical Origins of the Little Ice Age and Medieval Climate Anomaly. *Science*, **326**(5957), 1256–1260.

Marcott, S.A., Shakun, J.D., Clark, P.U., & Mix, A.C. 2013. A Reconstruction of Regional and Global Temperature for the Past 11,300 Years. *Science*, **339**(6124), 1198–1201.

Marzeion, B., Jarosch, A.H., & Hofer, M. 2012. Past and future sea-level change from the surface mass balance of glaciers. *The cryosphere*, **6**(6), 1295–1322.

Marzeion, B., Cogley, J.G., Richter, K., & Parkes, D. 2014. Attribution of global glacier mass loss to anthropogenic and natural causes. *Science*, **345**(6199), 919–921.

McGranahan, G., Balk, D., & Anderson, B. 2007. The rising tide: assessing the risks of climate change and human settlements in low elevation coastal zones. *Environment and urbanization*, **19**(1), 17–37.

Meier, M.F., Dyurgerov, M.B., Rick, U.K., O'Neel, S., Pfeffer, W.T., Anderson, R.S., Anderson, S.P., & Glazovsky, A.F. 2007. Glaciers Dominate Eustatic Sea-Level Rise in the 21st Century. *Science*, **317**(5841), 1064–1067.

Meinshausen, M., Raper, S.C.B., & Wigley, T.M.L. 2011. Emulating coupled atmosphere-ocean and carbon cycle models with a simpler model, MAGICC6 - Part 1: Model description and calibration. *Atmospheric chemistry and physics*, **11**(4), 1417–1456.

Mengel, M., & Levermann, A. 2014. Ice plug prevents irreversible discharge from East Antarctica. *Nature climate change*, **4**(6), 451–455.

Mitrovica, J.X., Gomez, N., Morrow, E., Hay, C.C., Latychev, K., & Tamisiea, M.E. 2011. On the robustness of predictions of sea level fingerprints. *Geophysical journal international*, **187**(2), 729–742.

Moore, J.C., Grinsted, A., & Jevrejeva, S. 2005. New tools for analyzing time series relationships and trends. *Eos trans. agu*, **86**(24).

Moore, J.C., Grinsted, A., Zwinger, T., & Jevrejeva, S. 2013. Semiempirical and process-based global sea level projections. *Reviews of geophysics*, **51**(3), 484–522.

Nerem, R. S., Chambers, D. P., Choe, C., & Mitchum, G. T. 2010. Estimating Mean Sea Level Change from the TOPEX and Jason Altimeter Missions. *Marine geodesy*, **33**(sup1), 435–446.

Nicholls, R.J., & Cazenave, A. 2010. Sea-Level Rise and Its Impact on Coastal Zones. *Science*, **328**(5985), 1517–1520.

Nicholls, R.J., Marinova, N., Lowe, J.A., Brown, S., Vellinga, P., de Gusmão, D., Hinkel, J., & Tol, R.S.J. 2011. Sea-level rise and its possible impacts given a 'beyond 4°C world' in the twenty-first century. *Philosophical transactions of the royal society a: Mathematical,physical and engineering sciences*, **369**(1934), 161–181.

Nick, F.M., Vieli, A., Andersen, M.L., Joughin, I., Payne, A., Edwards, T.L., Pattyn, F., & van de Wal, R.S.W. 2013. Future sea-level rise from Greenland's main outlet glaciers in a warming climate. *Nature*, **497**(7448), 235–238.

Orlić, M., & Pasarić, Z. 2013. Semi-empirical versus process-based sea-level projections for the twenty-first century. *Nature climate change*, **3**(8), 735–738.

PALSEA, PALeo SEA level working group. 2010. The sea-level conundrum: case studies from palaeo-archives. *Journal of quaternary science*, **25**(1), 19–25.

Peltier, W. Richard. 2002. On eustatic sea level history: Last Glacial Maximum to Holocene. *Quaternary science reviews*, **21**(1), 377–396.

Peltier, W.R. 2004. Global glacial isostasy and the surface of the ice-age Earth: The ICE-5G (VM2) model and GRACE. *Annual review of earth and planetary sciences*, **32**(1), 111–149.

Radić, V., & Hock, R. 2011. Regionally differentiated contribution of mountain glaciers and ice caps to future sea-level rise. *Nature geoscience*, **4**, 91–94.

Rahmstorf, S. 2007. A Semi-Empirical Approach to Projecting Future Sea-Level Rise. *Science*, **315**, 368 – 370.

Rahmstorf, S. 2010. A new view on sea level rise. *Nature reports climate change*, **4**(1004), 44–45.

Rahmstorf, S., Perrette, M., & Vermeer, M. 2011. Testing the robustness of semi-empirical sea level projections. *Climate dynamics*, **39**(3-4), 861–875.

Rahmstorf, S., Foster, G., & Cazenave, A. 2012. Comparing climate projections to observations up to 2011. *Environmental research letters*, **7**(4), 044035.

Rahmstorf, S., Box, J. E., Feulner, G., Mann, M.E., Robinson, A., Rutherford, S., & Schaffernicht, E.J. 2015. Exceptional twentieth-century slowdown in Atlantic Ocean overturning circulation. *Nature clim. change*, **5**(5), 475–480.

Rahmstorf, Stefan, Cazenave, Anny, Church, John A., Hansen, James E., Keeling, Ralph F., Parker, David E., & Somerville, Richard C. J. 2007. Recent Climate Observations Compared to Projections. *Science*, **316**(5825), 709–709.

Raper, S.C.B., & Braithwaite, R.J. 2005. The potential for sea level rise: New estimates from glacier and ice cap area and volume distributions. *Geophysical research letters*, **32**(5), n/a–n/a.

Ray, R.D., & Douglas, B.C. 2011. Experiments in reconstructing twentieth-century sea levels. *Progress in oceanography*, **91**(4), 496–515.

Reed, A.J., Mann, M.E., Emanuel, K.A., Lin, N., Horton, B.P., Kemp, A.C., & Donnelly, J.P. 2015. Increased threat of tropical cyclones and coastal flooding to New York City during the anthropogenic era. *Proceedings of the national academy of sciences*, **112**(41), 12610–12615.

Richardson, S.D., & Reynolds, J.M. 2000. An overview of glacial hazards in the Himalayas. *Quaternary international*, **65 66**, 31–47.

Rignot, E., Velicogna, I., van den Broeke, M.R., Monaghan, A., & Lenaerts, J. 2011. Acceleration of the contribution of the Greenland and Antarctic ice sheets to sea level rise. *Geophysical research letters*, **38**(5).

Roberts, E., & Andrei, S. 2015. The rising tide: migration as a response to loss and damage from sea level rise in vulnerable communities. *International journal of global warming*, **8**(2), 258–273.

Robinson, A., Calov, R., & Ganopolski, A. 2012. Multistability and critical thresholds of the Greenland ice sheet. *Nature climate change*, **2**(6), 429–432.

Rogelj, J., Meinshausen, M., & Knutti, R. 2012. Global warming under old and new scenarios using IPCC climate sensitivity range estimates. *Nature climate change*, **2**(4), 248–253.

Rohling, E.J., Haigh, I.D., Foster, G.L., Roberts, A.P., & Grant, K.M. 2013. A geological perspective on potential future sea-level rise. *Scientific reports*, **3**.

Rye, C.D., Naveira G., Alberto C., Holland, P.R., Meredith, M.P., George Nurser, A.J., Hughes, C.W., Coward, A.C., & Webb, D.J. 2014. Rapid sea-level rise along the Antarctic margins in response to increased glacial discharge. *Nature geoscience*, **7**(10), 732–735.

Schaeffer, M., Hare, W., Rahmstorf, S., & Vermeer, M. 2012. Long-term sea-level rise implied by 1.5°C and 2°C warming levels. *Nature climate change*, **2**(12), 867–870.

Schneider von Deimling, T., Ganopolski, A., Held, H., & Rahmstorf, S. 2006. How cold was the Last Glacial Maximum? *Geophysical research letters*, **33**(14), n/a–n/a.

Shakun, J.D., Clark, P.U., He, F., Marcott, S.A., Mix, A.C., Liu, Z., Otto-Bliesner, B., Schmittner, A., & Bard, E. 2012. Global warming preceded by increasing carbon dioxide concentrations during the last deglaciation. *Nature*, **484**(7392), 49–54.

Stanford, J.D., Hemingway, R., Rohling, E.J., Challenor, P.G., Medina-Elizalde, M., & Lester, A.J. 2011. Sea-level probability for the last deglaciation: A statistical analysis of far-field records. *Global and planetary change*, **79**(3-4), 193–203.

Storlazzi, C.D., Elias, E.P.L., & Berkowitz, P. 2015. Many Atolls May be Uninhabitable Within Decades Due to Climate Change. *Scientific reports*, **5**, 14546.

Törnqvist, T.E., & Hijma, M.P. 2012. Links between early Holocene ice-sheet decay, sea-level rise and abrupt climate change. *Nature geoscience*, **5**(9), 601–606.

Van den Broeke, Michiel R., Bamber, Jonathan, Lenaerts, Jan, & Rignot, Eric. 2011. Ice Sheets and Sea Level: Thinking Outside the Box. *Surveys in geophysics*, **32**(4-5), 495–505.

Van Vuuren, D.P., Edmonds, J., Kainuma, M., Riahi, K., Thomson, A., Hibbard, K., Hurtt, G.C., Kram, T., Krey, V., Lamarque, J.-F., Masui, T., Meinshausen, M., Nakicenovic, N., Smith, S.J., & Rose, S.K. 2011. The representative concentration pathways: an overview. *Climatic change*, **109**(1-2), 5–31.

Vermeer, M., & Rahmstorf, S. 2009. Global sea level linked to global temperature. *Proceedings of the national academy of sciences*, **106**(51), 21527–21532.

Vinther, B.M., Buchardt, S.L., Clausen, H.B., Dahl-Jensen, D., Johnsen, S.J., Fisher, D.A., Koerner, R.M., Raynaud, D., Lipenkov, V., Andersen, K.K., Blunier, T., Rasmussen, S.O., Steffensen, J.P., & Svensson, A.M. 2009. Holocene thinning of the Greenland ice sheet. *Nature*, **461**(7262), 385–388.

Wenzel, M., & Schröter, J. 2010. Reconstruction of regional mean sea level anomalies from tide gauges using neural networks. *Journal of geophysical research*, **115**(C8), C08013.

Wenzel, M., & Schröter, J. 2014. Global and regional sea level change during the 20th century. *Journal of geophysical research: Oceans*, **119**(11), 7493–7508.

Willis, J.K., & Church, J.A. 2012. Regional Sea-Level Projection. *Science*, **336**(6081), 550–551.

Winkelmann, R., Levermann, A., Martin, M.A., & Frieler, K. 2012. Increased future ice discharge from Antarctica owing to higher snowfall. *Nature*, **492**(7428), 239–242.

Woodruff, J.D., Irish, J.L., & Camargo, S.J. 2013. Coastal flooding by tropical cyclones and sea-level rise. *Nature*, **504**(7478), 44–52.

Woodworth, P.L., Morales Maqueda, M., Roussenov, V.M., Williams, R.G., & Hughes, C.W. 2014. Mean sea-level variability along the northeast American Atlantic coast and the roles of the wind and the overturning circulation. *Journal of geophysical research: Oceans*, **119**(12), 8916–8935.

Yin, J., & Goddard, P.B. 2013. Oceanic control of sea level rise patterns along the East Coast of the United States. *Geophysical research letters*, **40**(20), 5514–5520.

Zemp, M., et al. 2015. Historically unprecedented global glacier decline in the early 21st century. *Journal of glaciology*, **61**(228), 745–762.

Zwally, H.J., Li, J., Robbins, J.W., Saba, J.L., Yi, D., & Brenner, A.C. 2015. Mass gains of the Antarctic ice sheet exceed losses. *Journal of glaciology*, **advance online publication**.